ATLAS Note

ATL-ATLAS-CONF-2010-060

July 20, 2010

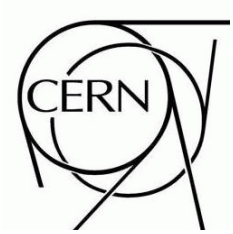

Luminosity Determination Using the ATLAS Detector

The ATLAS Collaboration

Abstract

We present the algorithms and results of the measurement of the luminosity in the ATLAS experiment during the first LHC run at energies of $\sqrt{s} = 900$ GeV and $\sqrt{s} = 7$ TeV. The LHC luminosity is determined in real time approximately once per second using a number of detectors and algorithms, each having different acceptances, systematic uncertainties and sensitivity to background. These results are displayed in the ATLAS control room and archived every two minutes; a single "preferred" measurement is reported to the LHC. During offline analysis, additional luminosity algorithms are studied and are compared to online results to further constrain systematic uncertainties on the measurement. Relative luminosities between detectors and methods in general agree to within a few per cent. Determination of the absolute luminosity using Monte Carlo calibrations is limited by a $\sim 20\%$ systematic uncertainty from the modeling of diffractive components of the cross section. Method-specific systematic uncertainties due to the modeling of detector response and trigger are $\sim 5\%$. Smaller uncertainties of 11% are obtained using an absolute calibration of the luminosity via beam separation scans and are dominated by the systematic uncertainty on the measurement of the LHC beam current. Monte Carlo based calibrations obtained using the PYTHIA MC09 (PHOJET) event generator differ from those obtained from the beam scans by 8% to 27% (26% to 35%).

A major goal of the ATLAS physics program for 2010 is the measurement of Standard Model cross sections. Accurate determination of luminosity is an essential ingredient of this program. We describe here the first results on luminosity determination, including an assessment of systematic uncertainties.

The note is organized as follows: Section 1 presents an overview of the ATLAS strategy for determining luminosity. Section 2 describes the ATLAS detectors and triggers used in this analysis. Section 3 defines the various algorithms used for luminosity determination. Section 4 describes the current status of luminosity measurements which use normalizations obtained from Monte Carlo. Section 5 discusses the absolute calibration of luminosity using beam scan data. Section 6 presents our conclusions.

1 Overview

The instantaneous luminosity of pp collisions can be calculated as:

$$\mathscr{L} = \frac{\mu n_b f_r}{\sigma_{inel}} = \frac{\mu^{meas} n_b f_r}{\varepsilon \sigma_{inel}} = \frac{\mu^{meas} n_b f_r}{\sigma_{vis}} \tag{1}$$

where μ is the average number of interactions per bunch crossing (BC), n_b is the number of bunches colliding at the interaction point (IP), f_r is the machine revolution frequency, σ_{inel} the inelastic cross section, ε is the efficiency of the luminosity algorithm (including the acceptance) for a certain detector, $\mu^{meas} = \varepsilon\mu$ is the average number of interactions per BC that pass the selection requirements of the algorithm and the "visible" cross section σ_{vis} is the detector calibration constant, which we will also refer to as the detector normalization. In general, Equation 1 is valid only in the case of a linear response of the detector with respect to μ, otherwise corrections for the non linearity of the detector response must be taken into account.

One of the challenges to this measurement is the large dynamic range of luminosity expected during the 2010-11 run (from 10^{26} cm^{-2}sec^{-1} obtained during the first fills at $\sqrt{s} = 900$ GeV, through the highest peak luminosity obtained to date[1)] of 2×10^{29} cm^{-2}sec^{-1}at $\sqrt{s} = 7$ TeV, to an expected 10^{32} cm^{-2}sec^{-1} by early 2011). Other challenges include the absence of measurements of the total pp inelastic cross section at either $\sqrt{s} = 900$ GeV or $\sqrt{s} = 7$ TeV, incomplete knowledge of the diffractive components of the inelastic cross section and the need to measure and remove machine-associated backgrounds. In addition, because real-time luminosity determination is an important tool for monitoring and optimizing LHC performance, ATLAS must produce accurate measurements during data collection and provide these measurements in real-time.

An important ingredient in the ATLAS program to control and understand systematic uncertainties in the luminosity measurements is the use of multiple detectors and multiple techniques and to monitor the degree to which these measurements track each other as a function of time. Since different approaches have different sensitivity to background and different correction factors as the mean number of interactions per beam crossing increases, any deviations in the reported luminosity obtained with different algorithms or detectors would indicate that at least one of the methods is inaccurate. Furthermore, since the different measurements have different sensitivity to the diffractive components of the pp cross section and depend on different detector acceptances, consistency among the measurements provides some level of validation of the Monte Carlo generator and simulation.

The LHC luminosity is determined in real time approximately once per second using a variety of detectors and algorithms that are described later in this note. These measurements are displayed in the ATLAS control room and results for a single "preferred" method is is sent to the LHC control room over the network, providing real-time feedback for machine tuning. The basic time unit for storing luminosity information for later use is the *Luminosity Block* (LB). The length of a LB is approximately two minutes,

[1)] The data samples used for this note contain data collected through July 19, 2010

with start and end times set by the ATLAS data acquisition system. All ATLAS data quality information, as well as luminosity, are stored in a relational database for each LB. Offline users therefore can select data samples with specific data quality requirements (for example, pixel detector ON) and then calculate the luminosity for that selection. Because the LB number is updated whenever a trigger prescale is changed and because trigger scalars are also recorded for each LB, offline users can correct the delivered luminosity for data acquisition deadtime and prescale rates. Furthermore, since the list of processed LB is included as in-file metadata for all ATLAS data formats, users can calculate the integrated luminosity properly for subsets of the full data sample.

The luminosity tables in the offline database allow for storage of multiple luminosity methods and are versioned so that updated calibration constants can be applied. All luminosity methods used online are stored, and results from additional offline algorithms are also available. This infrastructure makes it easy to compare the results from different methods as a function of time. After data quality checks have been performed and calibrations validated, one algorithm is chosen as the "preferred" offline algorithm for physics analysis and is stored as such in the database. Because the database tables allow multiple versions, new and improved calibration constants can be applied to previously taken data. Each time calibrations are updated a new database "tag" is declared.

Luminosity information is stored as *delivered* luminosity. Corrections for data acquisition deadtime and other sources of data loss are performed when the integrated luminosity is calculated. A tool is provided as part of the ATLAS software release that takes as its input the list of LB that have been analyzed (after data quality selection), the trigger used for the analysis (so that corrections for deadtime and trigger prescale can be made) and the luminosity method requested and returns the integrated luminosity of the data sample.

2 Detector Description

The ATLAS detector is described in detail in Reference [1]. We provide here brief descriptions of the subsystems used in the luminosity measurements presented in this note. ATLAS uses a coordinate system where the nominal interaction point is at the center of the detector, the beam direction defines the z-axis and the x-y plane is transverse to the beam. The positive x-axis is defined as pointing to the center of the ring and the positive y-axis is upwards. Side-A of the detector is in the positive z direction and side-C is in the negative z direction. The azimuthal angle ϕ is measured around the beam axis. The pseudorapidity η is defined as $\eta = -\ln(\tan\theta/2)$ where θ is the polar angle.

2.1 Minimum Bias Trigger Scintillators

For the initial running period at low luminosities ($< 10^{33}$ cm^{-2}s^{-1}), ATLAS has been equipped with segmented scintillator paddles, the Minimum Bias Trigger Scintillators (MBTS). The main purpose of the MBTS is to provide a trigger on minimum collision activity during a pp beam crossing (BC).

The MBTS detector consists of 32 scintillator paddles, 2 cm thick, organized into 2 disks, one on each side of the interaction point of ATLAS. The scintillators are installed on the inner face of the end-cap calorimeter cryostats, at $z = \pm$ 3560 mm, perpendicular to the beam direction. Each disk is separated into an inner and an outer ring, covering the radial regions $(153, 426)$ mm and $(426, 890)$ mm. In η these regions correspond to $(3.84, 2.82)$ and $(2.82, 2.09)$, respectively. Both the inner and the outer ring are organized into eight independent ϕ sectors, $2\pi/8$ radians wide. These sectors are placed such that the first sector has its edges at $\phi = 0$ and $\phi = \pi/4$ radians. Light emitted by each scintillator segment is collected by wavelength-shifting optical fibers and guided to a photomultiplier tube (PMT). The PMT signals are read out by the Tile Calorimeter (TileCal) electronics. The MBTS signals, after being shaped and amplified, are fed into leading edge discriminators and sent as 25 ns NIM pulses to the

Central Trigger Processor (CTP). An MBTS hit is defined as a signal above the discriminator threshold (30 mV).

2.2 LUCID

LUCID is a Cerenkov detector dedicated to measuring the luminosity in ATLAS. Sixteen mechanically polished aluminum tubes filled with C_4F_{10} gas surround the beampipe on each side of the interaction point at a distance of 17 m. The tubes are 1.5 m long and have a 15 mm diameter with a 1 mm wall thickness. The Cerenkov photons created by charged particles in the gas are reflected on the tube walls until they reach photomultipliers situated at the back end of the tubes. The photomultipliers have a 1.2 mm thick quartz window and a significant amount of Cerenkov light is also produced by particles in the windows. The aluminum tubes point towards the interaction point in order to reject particles that are not created directly in the pp-collisions, but since the primary particles pass through the beampipe at a very low angle the effective thickness of the beampipe is 15-20 cm and most particles recorded by LUCID are therefore secondary particles created in interactions in the beampipe or in the walls of the detector tubes.

The Cerenkov light created in the gas typically produces 60-70 photoelectrons while the quartz window adds another 40 photoelectrons to the signal. After amplification, the 32 signals are split three-fold and presented to a set of constant fraction discriminators (CFD), charge to digital convertors (QDC) and 32-bit flash ADCs (FADC) with 80 samplings. If the signal has a pulse height larger than the discriminator threshold (which is equivalent to 15 photoelectrons) a tube is said to have a hit and the hit-pattern produced by all the discriminators is sent to a purpose built electronics card (LUMAT) which contains FPGAs that can be programmed with different luminosity algorithms. LUMAT receives timing signals from the LHC clock used for synchronizing all detectors. It counts the number of events or hits passing each luminosity algorithm for each Bunch Crossing Identifier (BCID) in an orbit and also records the number of orbits made by the protons in the LHC during the counting interval. The data from the LUMAT card are made available online through the ATLAS information service (IS). In addition, LUMAT provides triggers for CTP and sends the hit-patterns to the ATLAS data acquisition (DAQ). The LUCID electronics is decoupled from the ATLAS DAQ so that it can provide an online luminosity determination even if no ATLAS DAQ run is in progress.

The data from LUCID are recorded in different ways. All events recorded by the central ATLAS DAQ contain the hit-pattern from the discriminators, as well as the LUCID trigger decisions. There is also a local data stream triggered by NIM logic that uses the discriminator signals as inputs and that requires at least one hit anywhere in the two detectors. This stream records the QDC and FADC values in addition to the CFD hit-pattern and stores these data in an independent data stream separate from the main ATLAS data. LUMAT data published through the IS are read by the online luminosity calculator (OLC). These data are also stored using the monitoring data archiving system (MDA) as histogram files. The histograms allow calculation of the luminosity per LB for each bunch crossing, as well as the luminosity averaged over all bunch crossings in the entire luminosity block. These histograms contain the number of empty events plus the number of hits for the different algorithms that are being used in LUMAT. At present there are four algorithms implemented in the LUMAT firmware (see Section 3.2).

2.3 Liquid Argon Calorimeter

The ATLAS electromagnetic calorimeters use liquid argon as the active detector medium. They consist of accordion-shaped absorbers and electrodes and are housed in three cryostats. The barrel cryostat contains the electromagnetic barrel calorimeter. The two endcaps (A and C) each contain an electromagnetic endcap calorimeter (EMEC), a hadronic endcap calorimeter (HEC), located behind the EMEC, and a forward calorimeter (FCAL). The EMEC consists of two co-axial wheels, an Outer Wheel covering the

rapidity range $1.375 < |\eta| < 2.5$ and an Inner Wheel covering the range $2.5 < |\eta| < 3.2$. The FCAL provides coverage over the range $3.1 < |\eta| < 4.9$. The luminosity analysis is based on energy deposits in the EMEC Inner Wheels and the FCAL, corresponding to the range $2.5 < |\eta| < 4.9$.

The electronics for the liquid argon calorimeters use an optimal-filtering method to calculate the energy for each calorimeter cell while minimizing the noise and pile-up contributions. The precise timing of the signal, as well as a χ^2-like quality factor, are determined and transmitted as well. This timing information is used to remove background in the offline measurement of luminosity using the Liquid Argon Calorimeter.

2.4 Inner Detector

The Inner Detector (ID) provides robust pattern recognition, excellent momentum resolution and measurements of primary and secondary vertices for charged tracks. The ID consists of three subsystems: a pixel detector, a silicon strip tracker (SCT) and a transition radiation straw tube tracker (TRT). These detectors cover a sensitive radial distance of 50.5-150 mm, 290-560 mm and 563-1055 mm respectively and cover a rapidity range $|\eta| < 2.5$. They are enclosed by a solenoidal magnet providing a 2 T axial field. The inner-detector barrel (end-cap) consists of 3 (2×3) Pixel layers, 4 (2×9) double-layers of single-sided silicon strips with a 40 mrad stereo angle and 73 (2×160) layers of TRT straws. The detectors have position resolutions of typically 10, 17 and 130 μm for the R-ϕ coordinates and in the case of the Pixel and SCT 115 and 580 μm for the second measured coordinate. A typical track traversing the barrel detector would leave 11 silicon hits (3 pixel clusters and 8 strip clusters) and more than 30 straw hits. Track reconstruction efficiencies as a function of transverse momentum (p_{T}) and rapidity are provided in reference [2]. The efficiency as a function of p_{T}, averaged over all rapidity, rises from $\sim$68% at 500 MeV to $\sim$92% at high momentum. The efficiency for $|\eta| < 1$, averaged over all p_{T} using a minimum bias spectrum for the momentum, is $\sim$ 85% . A relative systematic uncertainty of 4% is assigned to track reconstruction efficiency over most of the kinematic range, with larger uncertainties at the highest $|\eta|$ and lowest p_{T}. This uncertainty is dominated by possible inaccuracies in the Monte Carlo description of the material within the tracking volume and by the level of agreement between data and simulation.

2.5 Trigger

The ATLAS trigger consists of three levels of event selection: Level-1 (L1), Level-2 (L2), and event filter. The L2 and event filter together form the High-Level Trigger (HLT). The L1 trigger is implemented using custom-made electronics, while the HLT is almost entirely based on commercially available computers and networking hardware. The components of the trigger relevant for the luminosity analysis are the MBTS L1 triggers and the L1 random beam crossing trigger.

The ATLAS BPTX detectors use the same electrostatic beam pick-up system that the LHC uses to monitor the transverse position of the beam inside the beam pipe. The BPTX beam pick-up stations enable ATLAS to 'see' the particle bunches on their way towards the center of the experiment. They provide important reference-timing signals with respect to collisions, that are broadcast to all ATLAS subdetectors. The BPTX stations are located along the LHC on both sides of ATLAS, 175 m away from the interaction point. The signals from the BPTX stations are transmitted over 200 m low-loss cables to the ATLAS underground counting room (USA15). The BPTX signals are fed into the CTP to provide *filled-bunch triggers*.

The filled-bunch trigger is used by the CTP to identify the presence of bunches crossing at the ATLAS interaction point. During the 900 GeV running period, all physics triggers required that the filled-bunch trigger fire. For the 7 TeV running period, a new mechanism relying on the bunch-crossing identifier (BCID) has been used. Bunches that collide at the ATLAS IP are called "paired bunches." The BCID's

that correspond to such paired bunches are identified and grouped in a list called "physics bunch group", which is used to gate the physics triggers.

The MBTS physics triggers used to calculate the luminosity are the L1_MBTS_1_paired and the L1_MBTS_1_1_paired, which require respectively at least one hit in the MBTS and at least one hit in each of the A and C sides of the MBTS in a paired bunch trigger. To monitor and and correct for the presence of beam induced background, trigger items with the same logic but allowed to fired only in the BCIDs corresponding to unpaired bunches (L1_MBTS_1_unpaired and L1_MBTS_1_1_unpaired) are used.

2.6 Bunch-by-bunch luminosities and background estimation

The LHC beam is subdivided into 35640 RF-buckets of which nominally every tenth can contain a bunch. Subtracting abort and injection gaps, up to 2808 of these 3564 BCIDs can be filled. The BCID is stored as part of the ATLAS event record.

As noted above, LUCID can record the luminosity for each BCID separately and provide the result as LB-averages. Figure 1 shows the LUCID-measured luminosity for a 7 TeV run in which 13 BCIDs contained a bunch. Eight of these were colliding at IP1, four gave displaced collisions 11 m from IP1 and one bunch in each beam was unpaired. Comparison of the per-bunch luminosities provides an estimate of the background and of the signal purity and aids in the detailed understanding of the origin of the background.

When an algorithm that requires at least one hit in either LUCID arm is used, each displaced collision gives about 5% signal compared to one at the IP. The signal from the unpaired bunches is below 1 per-mil. Each real collision is followed by a long tail that can be attributed to slowly-decaying radiation background in the cavern. Before each collision signal, there is a small sub-per-mil peak due to the halo associated with the incoming beam. All these together add up to a background of about 6.3% in this particular run for a BCID-blind algorithm. If instead an algorithm that requires a coincidence between arms is used, the long tails (which are all random signals) are removed. The coincidence requirement also reduces the displaced collisions to about 1 per mil of the collisions at the IP and the signal from unpaired bunches becomes negligible. Thus a coincidence algorithm is preferable if a BCID-blind algorithm is used, especially if the fill contains displaced collisions. If only filled BCIDs are selected, however, then the single hit algorithm can also have very low background.

2.7 Online Luminosity Calculator

The task of the OLC is to retrieve the raw luminosity information (counts and number of LHC turns) from any subdetector and to apply the appropriate normalizations (determination of μ) and absolute calibrations. The OLC gets online information from the BPTX about the fill pattern in the LHC and uses this information in the luminosity normalization. For each luminosity algorithm, the OLC outputs instantaneous luminosities at about 1 Hz and calculates up to 4 different LB-average estimates, depending on what quantities are available for a given detector:

1. LBAv_all is a BCID-blind estimate as provided by the detector, e.g. the LUMAT card. This value is calculated without knowledge of which are BCIDs correspond to colliding bunches.

2. LBAv_phys is calculated if per-bunch luminosities are available, by selecting only the BCIDs matching the ATLAS physics bunch-group, i.e that collided at the ATLAS IP. By construction, this estimate is less susceptible to background than LBAv_all.

3. OLCLBAv_all is calculated by the OLC from the instantaneous values and serves as a fallback should LBAv_all not be available

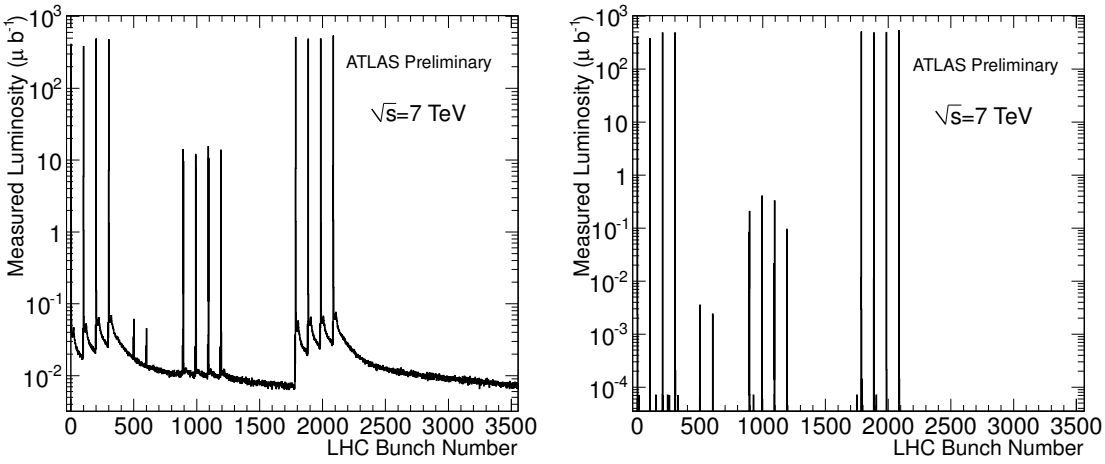

(a) (b)

Figure 1: Bunch-by-bunch LB-averaged luminosity in ATLAS run 155697 at 7 TeV, as recorded by an algorithm (left) that requires at least one hit in either LUCID arm, and by an algorithm (right) that requires a coincidence between at least one hit in each LUCID arm. The colliding BCIDs in this run were 1, 101, 201, 301, 1786, 1886, 1986 and 2086, BCIDs 895, 995 1095 and 1195 (of beam 1) had displaced collisions and BCIDs 601 (beam 1) and 501 (beam 2) were unpaired.

4. LBAv_perBunch is a vector of per-bunch luminosities, averaged over the LB.

The LB-average output of the OLC is stored in the ATLAS conditions database and displayed in the control room online. The instantaneous values are sent to online displays, stored in the ATLAS online-monitoring archive and shipped to the LHC control room over the network.

3 Overview of Methods of Determining Luminosity

Equation 1 gives the relationship between the luminosity $\mathscr{L}$, the average number of interactions per beam crossing μ and the "visible" cross section σ_{vis}. In this section, we describe the methods ATLAS uses to measure μ. The determination of σ_{vis} from Monte Carlo samples is discussed in Section 4. Determination of σ_{vis} from beam parameters (via the van der Meer scan method) is presented in Section 5.

3.1 MBTS

The MBTS is used to determine luminosity both online and offline. Online measurements are based on the information available to the CTP before any L1 trigger decision is taken. The online calculation is done using central trigger scalars counting the number of events for which any given L1 item fired. The counting time for each scalar is recorded by reporting the number of LHC turns. Every 10 s these counters are read out and made available online on the information service (IS), where they are retrieved by the OLC. For each LB, the counts are permanently stored in the ATLAS conditions database. There are three instances for each item: trigger before prescale (TBP), trigger after prescale (TAP), and trigger after veto (TAV). The trigger before prescale counts are calculated directly using inputs to the central trigger and are therefore free from any dead time or veto (as long as the deadtime is not 100%), while the trigger after veto corresponds to the rate of accepted events for which a trigger fired. Because the online luminosity calculation does not perform a background subtraction, the most reliable MBTS trigger to use for luminosity monitoring is the trigger with the lowest background rate, L1_MBTS_1_1_paired.

The offline event selection (MBTS_1_timing) begins with the same trigger requirements as the online, but uses the timing information in the MBTS to remove background. Figure 2 shows the time difference between the MBTS side A and side C ($\Delta t_{A,C}$) for the 900 GeV data and for simulation. The simulation reproduces the peak at $\Delta t_{A,C} = 0$ (which is attributed to particles arising from the collision point at the center of ATLAS). The secondary peaks at ± 24 ns corresponding to a round-trip distance of about 7.2 m are consistent with particles coming from upstream of ATLAS from beam-halo and beam-gas interactions. The Monte Carlo does not include interactions of this type. The offline selection requires a $|\Delta t_{A,C}| < 10$ ns cut. Using MC simulation we estimate the efficiency of this cut to be 0.986. The variation in selection efficiency changing the cut to 8 (12) ns is 0.976 (0.991) while the variation in the selection efficiency changing the center of the$|\Delta t_{A,C}| < 10$ ns distribution by ± 0.5 ns is smaller than 10^{-3}. To estimate the systematic effects introduced by a different time resolution in data and simulation the selection efficiency has been recalculated after having inflated the time resolution in simulation by 30%. The efficiency changed by less than 1%.

While the time resolution is well reproduced by the ATLAS simulation, the pulse height distributions in the MBTS are not well modeled. The effect of mis-modeling of the energy response has been studied by varying the MBTS response in the simulation to reflect the uncertainty on the calibrations. In addition, the efficiency has been measured in the data using an unbiased trigger that did not require the MBTS to fire. Based on these studies, an uncertainty of 7% (5%) for the 900 GeV (7 TeV) data is assigned to the trigger efficiency due to possible mis-modeling of the MBTS response.

Residual backgrounds in the L1_MBTS_1_1_paired sample have been evaluated. They include:

- *Cosmic rays:* the cosmic ray trigger rate has been measured to be $\sim 10^{-3}$ Hz using empty beam crossing triggers. Since the beam related L1_MBTS_1_1_paired rate was larger than 1 Hz even at the lowest luminosity of the 900 GeV running period and is significantly higher for the 7 TeV running period, this background is negligible.

- *Beam-induced backgrounds:* for the low luminosity 900 GeV running, backgrounds vary run-by-run and are subtracted using values obtained from the unpaired bunches, as show in Figure 3. In general, the backgrounds are low and are assigned a systematic uncertainty of 100% of the background size. For the 7 TeV running, the backgrounds after the timing cuts are very small ($< 10^{-4}$). Nevertheless, the background subtraction is still performed.

3.2 LUCID

Online luminosity values from LUCID measurements are obtained from the LUMAT card. At present there are four algorithms implemented in the LUMAT firmware:

- LUCID_Zero_AND, the number of events per BCID when no hits are found in either detector arm;
- LUCID_Zero_OR, the number of events per BCID when at least one of the two detector arms has no hits or when neither arm contains any hit;
- LUCID_Hit_AND, the number of hits when there is at least one hit in each of the two detector arms;
- LUCID_Hit_OR, the number of hits when there is at least one hit in the 32 tubes of both detector arms.

The counting of empty events was used in the analysis of the 2009 data but was converted to counts of non-empty events in the 2010 analysis simply because this is conceptually easier to understand. This was done by subtracting the number of empty events from the number of orbits to obtain:

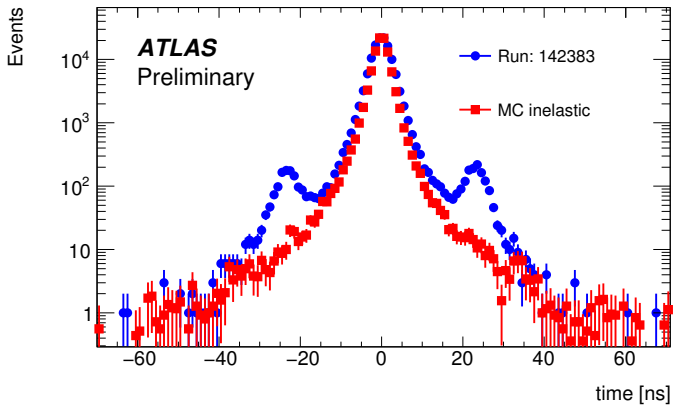

Figure 2: Time difference $\Delta t_{A,C}$ for L1_MBTS_1_1_paired selected events in run 142383 (blue circles) compared with MC simulation of inelastic processes (red squares). Data and simulation are normalized to the same number of events within $|\Delta t_{A,C}| < 10$ ns. The simulation includes only events from beam collisions, while the data also contains events from beam-halo background.

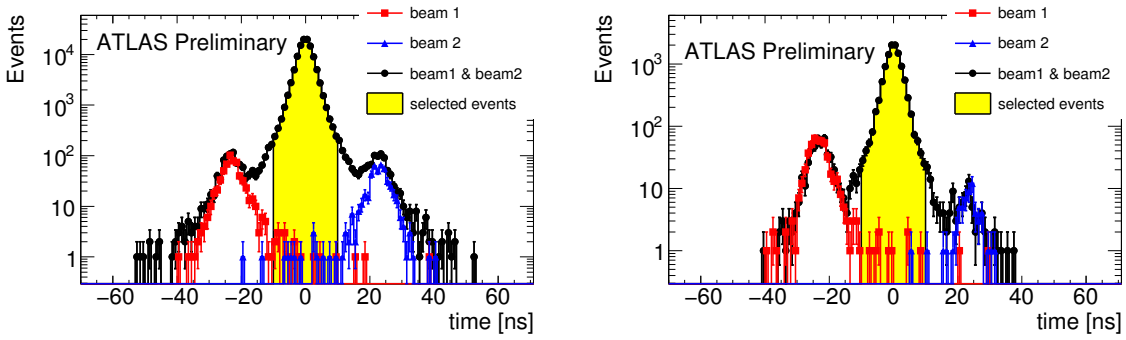

Figure 3: MBTS A-C side time difference $\Delta t_{A,C}$ for events triggered by the L1_MBTS_1_1_paired for the ATLAS runs 142193 and 142174. The circles (black) correspond to events selected with L1_MBTS_1_1_paired, the shaded (yellow) area defines the events passing the $|\Delta t(A-C)| < 10$ ns requirement, the triangles (blue) correspond to the Beam-Halo background of beam 2, and the squares (red) correspond to the Beam-Halo background of beam 1. The Beam-Halo background has been extracted by looking at the unpaired BCID separately for beam 1 and beam 2. The background normalization is fixed to the ratio of the beam current carried by the paired bunches to that in the unpaired bunches.

- LUCID_Event_AND, the number of events with at least one hit in each detector arm. The LUCID_Event_AND probability per beam crossing $P^{\text{LUCID\_Event\_AND}}$ is related to the LUCID_Zero_OR probability per beam crossing $P^{\text{LUCID\_Zero\_OR}}$:

$$P^{\text{LUCID\_Event\_AND}} = 1 - P^{\text{LUCID\_Zero\_OR}}$$

- LUCID_Event_OR, the number of events for which the sum of hits in both detector arms is larger or equal to one. The LUCID_Event_OR probability per beam crossing $P^{\text{LUCID\_Event\_OR}}$ is related to the LUCID_Zero_AND probability per beam crossing $P^{\text{LUCID\_Zero\_AND}}$:

$$P^{\text{LUCID\_Event\_OR}} = 1 - P^{\text{LUCID\_Zero\_AND}}$$

The event counting methods are generally more precise than the hit counting methods as long as the average number of interactions per bunch crossing (μ) is small; therefore event counting has been used to calculate the luminosity, while the hit counting algorithms have so far been used mainly for consistency checks. The hit counting methods will, however, be an important tool when the luminosity increases since they do not saturate as quickly as event counting methods. As long as the background is small, LUCID_Event_OR counting is also usually preferable to LUCID_Event_AND counting since it gives a smaller statistical uncertainty and a less complicated dependence on the number of interactions per bunch crossing (see Section 3.5).

From this discussion it is clear that the most accurate method of determining luminosity with LUCID is the LUCID_Event_OR if the background is not a problem. When LHC started running, it was a completely open question what background levels to expect. It was a pleasant surprise that the background in the LUCID_Event_AND sample is negligible, and that it is small in the LUCID_Event_OR sample, both at 900 GeV and at 7 TeV, as long as one retains only the luminosity counts from the paired bunches. This background was evaluated using the unpaired bunches in order to account for beam-related effects (beam-halo and beam-gas). The number of events in the unpaired bunches was counted and scaled, taking into account the ratio of paired to unpaired bunches and their bunch currents. At 900 GeV, where the luminosity was quite low, the background was measured to be $< 3\%$ for all fills. Results of this study for a typical run at 7 TeV are shown in Figure 4. The background is typically 10^{-4} for the LUCID_Event_OR trigger and $< 10^{-5}$ for the LUCID_Event_AND trigger. Contributions from other sources such as cosmic rays and electronic noise have been measured in the absence of beam and are negligible when selecting only the colliding BCIDs.

The low average hit-multiplicity at 900 GeV made it very difficult to calculate the efficiencies with an uncertainty better than 30% using simulation. It was decided instead to obtain the LUCID efficiencies by counting LUCID and MBTS events in one long run (using a sample that satisfies a trigger that does not depend on the requirement that either LUCID or MBTS fire), and then to use the Monte Carlo determined efficiency for the L1_MBTS_1_1_paired trigger:

$$\varepsilon_{LUCID} = \frac{n_{LUCID}}{n_{\text{L1\_MBTS\_1\_1\_paired}}} \cdot \varepsilon_{\text{L1\_MBTS\_1\_1\_paired}}$$

This means that the overall luminosity scale for 900 GeV data is identical for LUCID and MBTS and that only the time dependence of the luminosity calculated by the two detectors can be compared. The method depends on the assumption that the efficiencies for finding hits in LUCID and in MBTS are not biased by the trigger selected for this study.[2)]

For the 7 TeV running, the average hit-multiplicity is high enough for the LUCID simulation to provide an accurate estimation of the efficiency for the LUCID_Event_OR method. The results of this

[2)] The low instantaneous luminosity of the 2009 900 GeV run precluded the use of a random trigger.

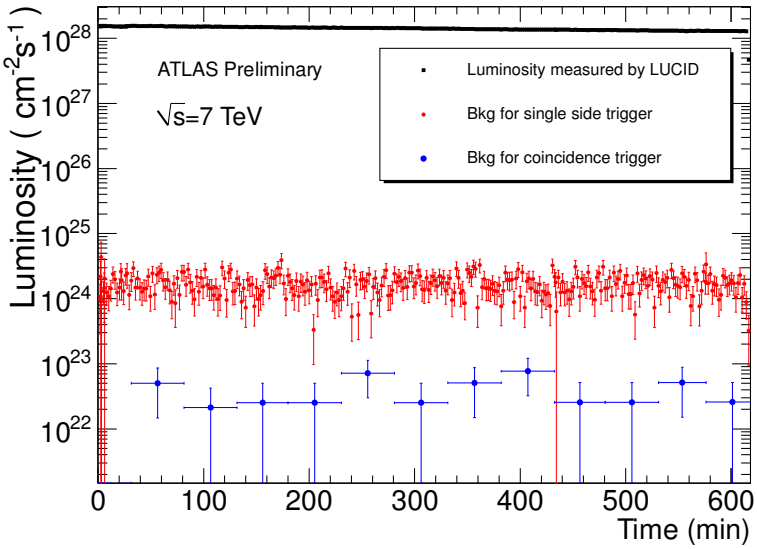

Figure 4: The luminosity measured by LUCID at 7 TeV for one LHC fill obtained from paired bunches is displayed together with the background level for the single-sided LUCID_Event_OR and for the coincidence LUCID_Event_AND triggers. The background has been calculated from unpaired bunches.

efficiency calibration is used to compare LUCID with measurements by other detectors. In addition, calibrations were done using MBTS in the same way as in 2009 and cross checks were made with the Liquid Argon luminosity calculation (described in Section 3.3). It was decided that because of the higher average hit-multiplicity in MBTS, a calibration using MBTS events and the Monte Carlo determined MBTS efficiency would most likely provide the most accurate calibration. Therefore, this choice was used for both the recorded online and offline luminosity with LUCID.

3.3 Liquid Argon Calorimeter Endcaps

The measurement of luminosity using the Liquid Argon endcap calorimeters is performed by analyzing minimum bias data offline. Events are required to pass the L1_MBTS_1_paired trigger and the rate of events with significant in-time energy deposits in both EM calorimeter endcaps is then measured. The analysis considers the energy deposits in the EMEC Inner Wheels and the FCAL, corresponding to the pseudorapidity range $2.5 < |\eta| < 4.9$. Cells are required to have an energy 5σ above the noise level and to have $E > 250$ MeV in the EMEC or $E > 1200$ MeV in the FCAL. Two cells passing these requirements are required on both the A- and the C-side. The time on e.g. the A-side is then defined as the average time of all the cells on the A-side that pass the above requirements.

The distribution of the LAr endcap timing difference is shown for two example runs in Fig. 5. In both runs there is a clear peak at $\Delta t_{\mathrm{LArEC}} \approx 0$ which is attributed to particles arising from the collision point at the center of ATLAS. There are secondary peaks at ± 30 ns corresponding to a distance of about 9 m, consistent with particles coming from upstream of ATLAS (e.g. due to a beam-gas interaction) and then traversing both endcaps. The events in these satellite peaks are background to the luminosity measurement: for the analysis a cut of ± 5 ns is placed to reject this background. It is seen in Fig. 5 that in run 142383 there is very little background while the background is significant for run 142406. The background that remains after the $|\Delta t_{LArEC}| < 5$ ns cut can be estimated from the activity in the non-colliding bunches. During most of the data-taking the background rate is below 0.05 Hz. For most runs

at 900 GeV, this corresponds to a background fraction well below 1% . At 7 TeV, where the instantaneous luminosity is higher, the backgrounds are typically of order 10^{-4}.

Fig. 5 also shows the distribution for simulation. It is seen that there is a slight shift between data and simulation. The data mean value is +0.73 ns for both runs while the simulation peaks at 0. The slight shift in the data is consistent with the current expected timing precision of about 1 ns. The width is in good agreement between data and simulation.

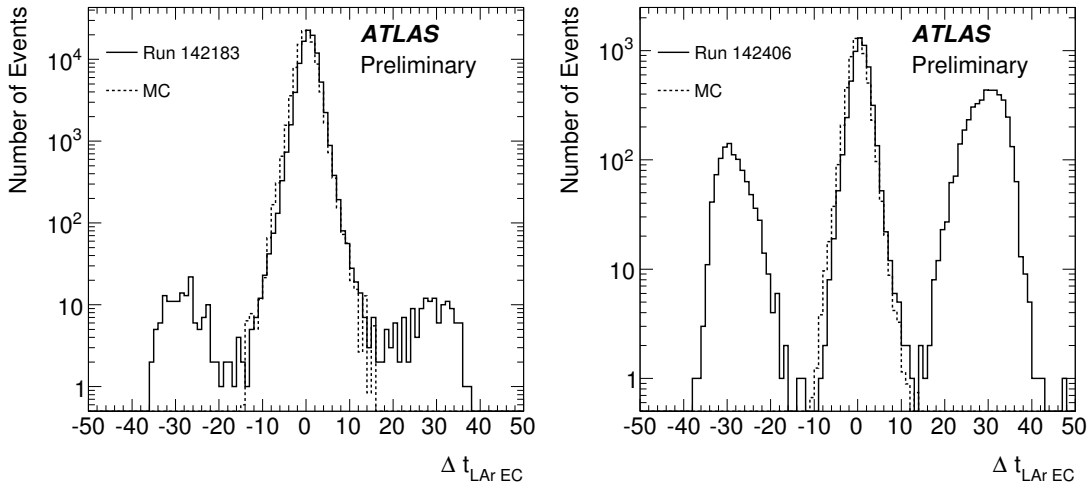

Figure 5: The difference in ns between the arrival time of the signal in the LAr calorimeter endcaps A and C for ATLAS runs 142193 and 142406.

For events passing the Liquid Argon selection, including the timing cut, the L1_MBTS_1_paired efficiency is 100% in the Monte Carlo. A random L1_BPTX beam crossing trigger is used to verify this L1_MBTS_1_paired efficiency. In the 900 GeV data collected in 2009, 74 events were found that satisfy the timing cut, and all of these events are triggered by the L1_MBTS_1_paired trigger. Studies at 7 TeV confirm that the MBTS trigger is fully efficient for events passing the Liquid Argon selection. For this analysis an efficiency of 100% is used for the L1_MBTS_1_paired trigger. A systematic uncertainty of 2% is assigned to this efficiency to reflect the limited statistical power of the L1_BPTX measurement and the intrinsic uncertainties in the accuracy of the simulation.

The L1_BPTX trigger was also used to estimate the background rate. At 900 GeV, the background is measured to be $< 1\%$. At 7 TeV, one run containing 1.3 million L1_MBTS_1_paired triggered events found no events in the unpaired bunch trigger. After correcting for trigger prescales, this result sets a conservative limit on the background rate of 10^{-4}.

3.4 Charged Particle Event Counting

Measurements of the luminosity have been performed offline by counting the rate of events with a reconstructed primary vertex in the L1_MBTS_1_paired trigger sample. Two variants of this analysis have been implemented that differ only in the details of the primary vertex reconstruction and the momentum and fiducial cuts applied to the reconstructed tracks.

The first analysis, referred to here as *charged particle event counting* has selection criteria agreed to by the LHC Rate-Normalization Task Force and is designed to allow the comparison of results from ALICE, ATLAS and CMS. The method counts the rate of events that have at least one track with transverse momentum $p_T > 0.5$ GeV and pseudorapidity $|\eta| < 0.8$. The track selection and acceptance corrections

used in this analysis are identical (with the exception of the $|\eta| < 0.8$ requirement) to those used in ATLAS's published 900 GeV minimum bias analysis [2]. The main criteria are that the L1_MBTS_1_paired trigger be satisfied, that a primary vertex with at least three tracks with $p_T > 150$ MeV be reconstructed and that there be at least one track with $p_T > 500$ MeV, $|\eta| < 0.8$ and at least 6 SCT hits and one pixel hit. Data are corrected for the trigger efficiency, the efficiency of the vertex requirement and the tracking efficiency (which is a function of both p_{T} and η). For this event selection, the vertex efficiency is 95% for events with only one charged particle above 0.5 GeV and nearly 100% for higher multiplicity. The trigger efficiency for this selection is close to 100%. The loss of events due to tracking inefficiencies is obtained using a correction factor C that depends on the charged multiplicity n_{ch}:

$$C(n_{ch}) = \frac{1}{1-(1-<\varepsilon>)^{n_{ch}}}$$

where the average tracking efficiency $<\varepsilon>$ over the acceptance region is 85% (where the efficiency has been calculated using a PYTHIA MC09 [3] minimum bias Monte Carlo sample). The number of events with $n_{ch} > 0$ is then obtained by integration. This analysis has only been performed on the $\sqrt{s} = 900$ GeV sample.

The second analysis, referred to here as *primary vertex counting* has larger acceptance. The track and vertex reconstruction cuts used are identical to those used by ATLAS for its study of charged particle multiplicities at $\sqrt{s} = 7$ TeV [4]. An offline reconstructed primary vertex is required, formed starting from at least two tracks with $p_T > 100$ MeV, as reconstructed in the ATLAS inner tracking detector. The tracks are required to fulfill the following quality requirements: transverse impact parameter computed with respect to the beam spot center $|d_0| < 4$ mm, errors on the transverse and longitudinal impact parameters $\sigma(d_0) < 5$ mm and $\sigma(z_0) < 10$ mm, at least 4 hits in the SCT, at least 6 hits in Pixel and SCT. These requirements lead to an efficiency of $83.5 \pm 0.1\%$, as estimated from ATLAS simulation using events generated with the PYTHIA MC09 tune.

3.5 Determining μ from N

For all of the methods described above, the relationship between N and μ exhibits non-linearities at large μ. Corrections for such non-linearities depend on the efficiency for an inelastic event to pass the specified selection criteria. The form of the correction is different for algorithms that require a single hit or reconstructed object in the event (eg the LUCID_Event_OR or L1_MBTS_1_paired) and for those that require a coincidence between both sides of the detector (eg the LUCID_Event_AND or L1_MBTS_1_1_paired).

As noted in section 3.2, the zero counting (Zero_AND) method is equivalent to the method that requires at least one hit in either detector (Event_OR) for any detector system. The probability to observe such an event if the average number of interactions per beam crossing is μ can be obtained using Poisson statistics and the efficiency ε for finding a hit or object satisfying our criteria in an inelastic pp collision. The resulting expression is an exponential

$$P^{ZERO-AND} = e^{-\varepsilon\mu}$$

In order to determine the luminosity this expression has to be inverted and for the ZERO-AND algorithm, in which one wants to convert the number of empty bunch crossings into the average number of interactions per colliding bunch crossing (BCID), the following formula is obtained:

$$\mu_{ZERO-AND} = -\frac{1}{\varepsilon} \cdot \ln\left(\frac{N^{zero-and}}{n_b \times N^{orbits}}\right) \quad (2)$$

The instantaneous luminosity is then obtained as:

$$\mathscr{L} = \sum_{i \in BCID} \mu_i \frac{f_r}{\sigma_{vis}} \tag{3}$$

where the sum is performed over the colliding BCIDs.

For methods requiring a coincidence between sides, the situation is a bit more complicated, since the probability in this case depends on three exponentials and three parameters (the probability of detecting an interaction on side A (ε_A), the probability of detecting an interaction on side C (ε_C), and the probability of detecting a coincidence between the two sides, (ε_{coinc})) which results in an expression that cannot be inverted analytically. Approximations can, however, be made for low μ values. LUCID, for example, assumes a linear approximation for the online luminosity calculation, which is correct to within 5% up to a μ-value of 2. The formula for the LUCID_Event_AND method becomes:

$$\mu_{\text{LUCID\_Event\_AND}} = \frac{1}{\varepsilon_{\text{LUCID\_Event\_AND}}} \cdot \frac{N^{\text{Zero\_Or}}}{n_b \times N^{orbits}} \tag{4}$$

Analysis of the van der Meer data used the full expressions for the μ dependence rather than the linear approximation.

The MBTS, which has higher efficiency, determines the online luminosity using a logarithmic approximation based on Equation 2, but setting the efficiency ε equal to the efficiency for observing at least one hit in each MBTS side.

It should be noted that once the single arm and double arm visible cross sections are determined from van der Meer scan data, the expressions for the μ dependence can be written in terms of these cross sections, removing the need to rely on Monte Carlo determined efficiencies.

4 Luminosity Determination Using Monte Carlo Derived Calibrations

4.1 Cross Sections and Efficiencies

At the Tevatron, luminosity measurements were normalized to the inclusive, inelastic $p\bar{p}$ cross section, with simulated data used to determine the zero-counting or hit-counting efficiencies [5] [6]. ATLAS has used a similar technique. The luminosity is calculated as:

$$\mathscr{L} = \frac{\mu^{meas} n_b f_r}{\sigma_{vis}} = \frac{\mu^{meas} n_b f_r}{\varepsilon_{ND}\sigma_{ND} + \varepsilon_{SD}\sigma_{SD} + \varepsilon_{DD}\sigma_{DD}} \tag{5}$$

where $\varepsilon_{process}$ are the efficiencies and $\sigma_{process}$ the cross sections for the individual inelastic processes contributing. These processes are non-diffractive (ND), single-diffractive (SD), and double-diffractive (DD).

Unlike the case of the Tevatron, where the $p\bar{p}$ cross section was determined independently by two experiments [6][3)], the pp cross sections at 900 GeV and 7 TeV have not been measured. In addition, at the Tevatron measurements of the diffractive components of the cross section were performed using a Roman-pot system. Such measurements are not currently available for ATLAS. In the future, studies of rapidity gaps in minimum bias events will help in calculating the rate for and characterizing the properties of diffractive events. In addition, the ALFA detector [7] will provide an absolute luminosity calibration through the measurement of elastic pp-scattering at small angles in the Coulomb-Nuclear Interference (CNI) region. Until such additional measurements are made, Monte Carlo based calibration

[3)] In fact, Tevatron cross sections were measured at $\sqrt{s} = 1.8$ TeV and extrapolated to $\sqrt{s} = 1.96$ TeV

$\sqrt{s} = 900$ GeV		
Process	PYTHIA	PHOJET
non-diffractive	34.4	40.0
single-diffractive	11.7	10.5
double-diffractive	6.4	3.5
Total:	52.5	54.0

$\sqrt{s} = 7$ TeV		
Process	PYTHIA	PHOJET
non-diffractive (ND)	48.5	61.6
single-diffractive (SD)	13.7	10.7
double-diffractive (DD)	9.3	3.9
Total:	71.5	76.2

Table 1: Predicted inelastic pp cross sections in mb at $\sqrt{s} = 900$ GeV and $\sqrt{s} = 7$ TeV for PYTHIA and for PHOJET. Note: A small ~ 1 mb contribution from double pomeron processes ("central diffraction") was not included in the PHOJET cross section.

of the absolute luminosity that rely on the modeling of the inelastic cross section will incur a significant systematic uncertainty.

One indication of the size of this uncertainty can be obtained by comparing the cross sections and acceptances obtained with two Monte Carlos: PYTHIA (using the ATLAS MC09 tune) and PHOJET. Table 1 shows the PYTHIA and PHOJET predictions for the inelastic cross sections at $\sqrt{s} = 900$ GeV and $\sqrt{s} = 7$ TeV. The predicted cross section in PHOJET are higher than PYTHIA by 3% at 900 GeV and 6.5% at 7 TeV. Table 2 shows the predicted efficiencies for observing ND, SD and DD events for the different methods ATLAS uses for luminosity determination. While the efficiency for observing ND events are similar for the two generators, the efficiency for observing diffractive events is quite different. This can be explained in terms of the different predictions for the multiplicity, p_{T} and η distributions for particles produced in the diffractive processes. It should be noted that there is no guarantee that these generators (and the specific generator tunes chosen here) span the space of predictions. Thus, estimates of the systematic uncertainty for the Monte Carlo based normalization of the luminosity are difficult to assess fully.

4.2 Absolute and Relative Luminosity Measurements

ATLAS normalizes its Monte Carlo based luminosity measurements using the PYTHIA prediction for the inelastic cross section (52.5 mb at 900 GeV and 71.5 mb at 7 TeV). Each measurement uses a value of σ_{vis} determined using PYTHIA tune MC09 and assigns a systematic uncertainty of $\sim 20\%$ due to the dependence of the efficiency on the choice of Monte Carlo generator. This dependence results from differences in assumed diffractive cross sections, differences in the predicted distributions of particle multiplicity and momentum, and differences in the short- and long-range correlations among particles. The uncertainty common to all methods is significantly larger than the uncorrelated method-specific systematic uncertainties that can be attributed to uncertainties in detector response. The systematic uncertainties at $\sqrt{s} = 900$ GeV (7 TeV) for each of the methods used to determine absolute luminosity are summarized in Table 3 (Table 4).

The performance of these algorithms at $\sqrt{s} = 900$ GeV ($\sqrt{s} = 7$ TeV) is shown in Figures 6 and 7 (8 and 9). Figure 6 shows the comparison of the instantaneous luminosities as a function of time for one 900 GeV run obtained using the Liquid Argon, MBTS and charged particle event counting methods. For each of these measurements, the acceptance is independently calculated using PYTHIA. As discussed in Section 3.2, the multiplicity in LUCID at 900 GeV was too low to obtain reliable calibration constants, so LUCID is not included in this comparison. The luminosity obtained with the charged particle event counting method is about 10% higher than that obtained from the Liquid Argon and a few per cent higher than that obtained from the MBTS. Figure 7 compares the instantaneous luminosities for the same run, but normalizing the LUCID_Event_OR and Liquid Argon results to give the same luminosity as the MBTS (integrated over the run).

MBTS_1_timing				
	900 GeV		7 TeV	
Process	Efficiency (%)		Efficiency (%)	
	PYTHIA MC09	PHOJET	PYTHIA MC09	PHOJET
ND	95.2	95.3	97.4	97.9
SD	26.7	32.8	41.3	44.3
DD	38.7	66.4	50.8	68.1
σ_{vis} (mb)	38.4	42.9	57.6	67.8

Liquid Argon				
	900 GeV		7 TeV	
Process	Efficiency (%)		Efficiency (%)	
	PYTHIA MC09	PHOJET	PYTHIA MC09	PHOJET
ND	90.2	88.6	96.0	94.3
SD	11.3	17.1	21.4	27.9
DD	22.7	60.0	25.9	53.6
σ_{vis} (mb)	33.8	39.4	51.9	63.2

	Charged Particle Event Counting		Primary Vertex Counting	
	900 GeV		7 TeV	
Process	Efficiency (%)		Efficiency (%)	
	PYTHIA MC09	PHOJET	PYTHIA MC09	PHOJET
ND	76	75	97.8	99.2
SD	17	38	43.9	56.9
DD	16	39	47.8	70.7
σ_{vis} (mb)	29.2	35.4	57.9	70.0

	LUCID_Event_OR		LUCID_Event_AND	
	7 TeV		7 TeV	
Process	Efficiency (%)		Efficiency (%)	
	PYTHIA MC09	PHOJET	PYTHIA MC09	PHOJET
ND	79.2	74.2	30.8	25.5
SD	28.7	44.8	1.2	2.4
DD	39.4	62.0	4.4	14.8
σ_{vis} (mb)	46.1	52.9	15.5	16.4

Table 2: Efficiency at $\sqrt{s} = 900$ GeV and $\sqrt{s} = 7$ TeV for the various luminosity methods described in Section 3. The σ_{vis} is obtained from Equation 5 using these acceptances and the cross sections from Table 1. Note: no numbers are provided for LUCID for $\sqrt{s} = 900$ GeV because the low average hit-multiplicity at this energy made it difficult to calculate the efficiency with an uncertainty of $< 30\%$.

Systematic Uncertainty $\sqrt{s} = 900$ GeV				
Source	Liquid Argon (%)	MBTS_1_timing (%)	Charged Particle (%)	Correlation (%)
σ_{vis}	18	15	20	fully correlated
Detector response	5.5	n.a	2	uncorrelated
Background	$< 1\%$	$< 1\%$	$< 1\%$	uncorrelated
Trigger Efficiency	2	7	2	fully correlated
Total	21	17	20	highly correlated

Table 3: Systematic uncertainties on the Monte Carlo based calibration of luminosity at $\sqrt{s}$ =900 GeV. The last column indicates whether the uncertainty is correlated among the measurements.

Systematic Uncertainty $\sqrt{s} = 7$ TeV				
Source	Liquid Argon (%)	MBTS_1_timing (%)	LUCID (AND or OR) (%)	Correlation (%)
σ_{vis}	20	20	20	100
Detector response	5.5	n.a	5.0	0
Background	negligible	negligible	negligible	0
Trigger Efficiency	2	5	n.a	100
Total	21	21	20	100

Table 4: Systematic uncertainties on the Monte Carlo based calibration of luminosity at $\sqrt{s}$ =7 TeV. The last column indicates whether the uncertainty is correlated among the measurements.

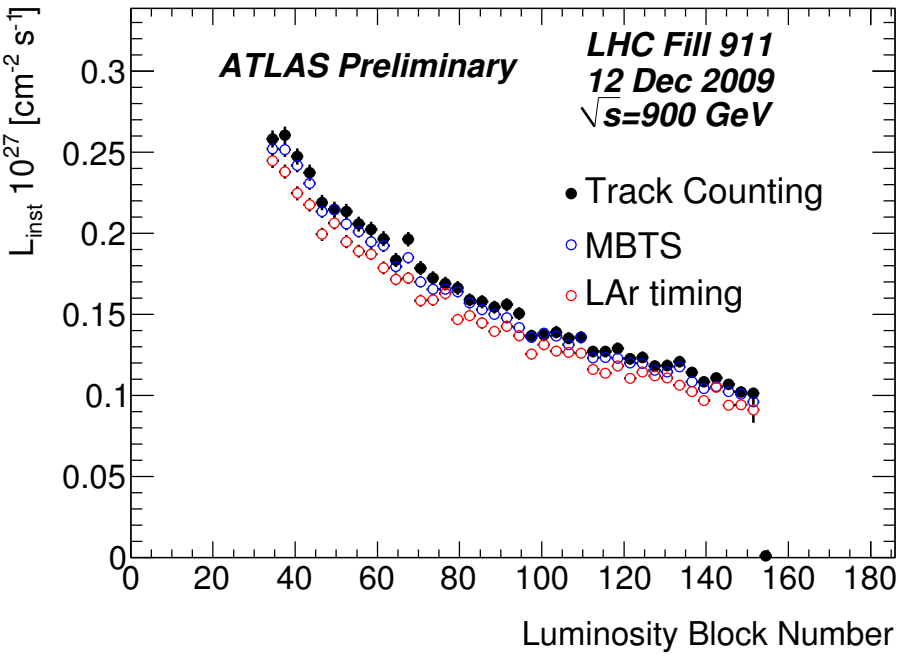

Figure 6: Comparison of the instantaneous luminosity obtained using the Liquid Argon, MBTS and charged particle event counting methods for run 142193, taken by ATLAS on Dec 12, 2009 at $\sqrt{s} =$ 900 GeV. For each of these measurements, the acceptance is independently calculated using the PYTHIA Monte Carlo simulation of the pp inelastic interactions.

The instantaneous luminosity calculated with independent calibrations is shown in Figure 8 for one 7 TeV run. At this energy the multiplicity in LUCID is high enough to allow Monte Carlo calibration and it is therefore included in the figure. At 7 TeV the MBTS and Liquid Argon results are consistent to better than 1%. The results for LUCID_Event_OR are consistent with MBTS and Liquid Argon to $\sim 3\%$. Figure 9 shows the instantaneous luminosity for the same run with the Liquid Argon and LUCID luminosities normalized to that of the MBTS (integrated over the run). The relative luminosity of these methods track each other within the statistical uncertainties of the algorithms.

5 Absolute Calibration Using Beam-Separation Scans

It is clear from the discussion in Section 4 that the systematic uncertainty on the luminosity determination will remain large as long as ATLAS is dependent on Monte Carlo models of total pp inelastic processes to determine the visible cross section. In the future, when much larger integrated luminosities are recorded, it may be possible to normalize cross-section measurements to electroweak processes for which precise NNLO calculations exist, for example W production [8]. At present, an attractive alternative is to determine the absolute luminosity by using machine parameters, which does not require the *a priori* knowledge of any cross-section. The method is known as *van der Meer (vdM)* scans, sometimes also called *beam-separation* or *luminosity* scans. This method was invented by S. van der Meer in 1968 [9] who found that it was possible to measure the effective height of the colliding *ISR* beams by observing the counting rate R in a suitable detector while scanning one of the two beams in the vertical plane with respect to the other one. The measurement of the counting rate versus displacement would yield a bell-shaped curve with its maximum at zero displacement. As will be detailed in Section 5.3, the

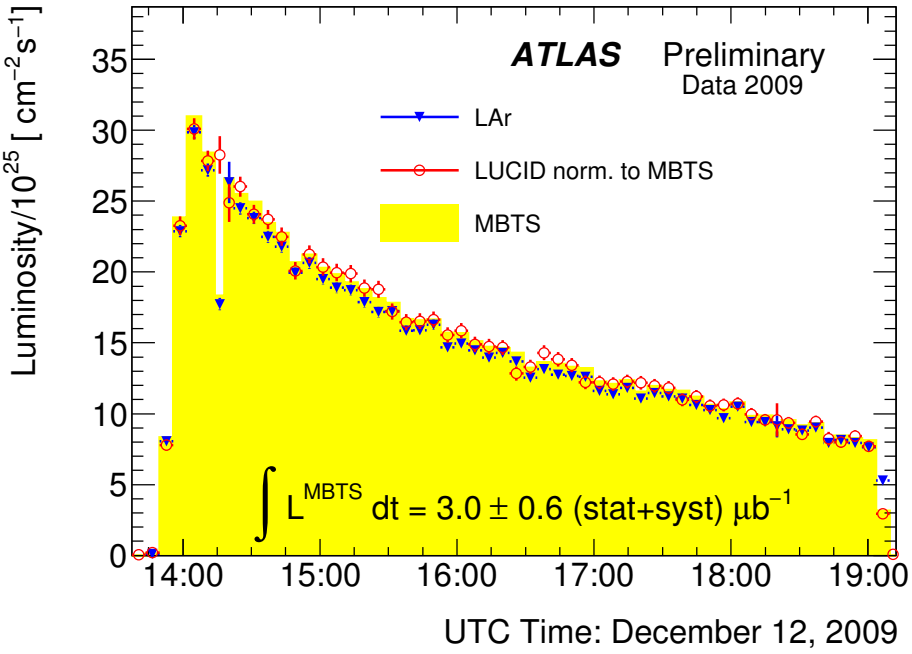

Figure 7: Instantaneous luminosity determined by three independent methods for run 142193, taken by ATLAS on Dec 12, 2009. This run offered an extended stable-beam period of 4.5 hours at $\sqrt{s} = 900$ GeV, thus allowing ATLAS to measure the instantaneous luminosity for varying beam intensities. The plot shows the performance of the LAr and LUCID_Event_OR normalized to give the same integrated luminosity as the MBTS results. The MBTS (shaded area) result provides the ATLAS luminosity. It is corrected for the dead time in the data acquisition system, and is therefore an estimate of the LHC delivered luminosity at the ATLAS interaction point. At time 14:16, the ATLAS data acquisition system suffered 100% dead time, making it impossible to properly correct the MBTS luminosity. The LUCID detector readout is decoupled from the ATLAS data acquisition system and was not affected by this problem.

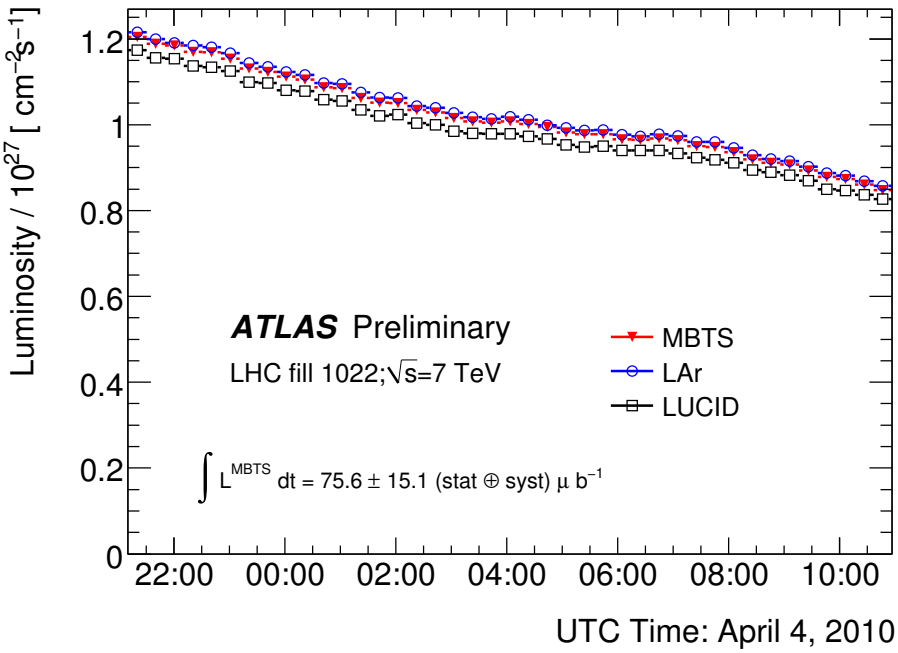

Figure 8: The ATLAS instantaneous luminosity as determined with the LAr (blue open circles), the LUCID_Event_OR (open squares), and MBTS (red triangles) sub-detectors for ATLAS run 152409, taken at $\sqrt{s} = 7$ TeV. The LAr instantaneous luminosity is corrected for the dead time in the data acquisition system, and therefore is an estimate of the LHC delivered luminosity at the ATLAS interaction point. Neither the MBTS nor the LUCID method are affected by data-acquisition dead time. For each of these measurements the acceptance is independently calculated using the PYTHIA Monte Carlo simulation of the pp inelastic interactions.

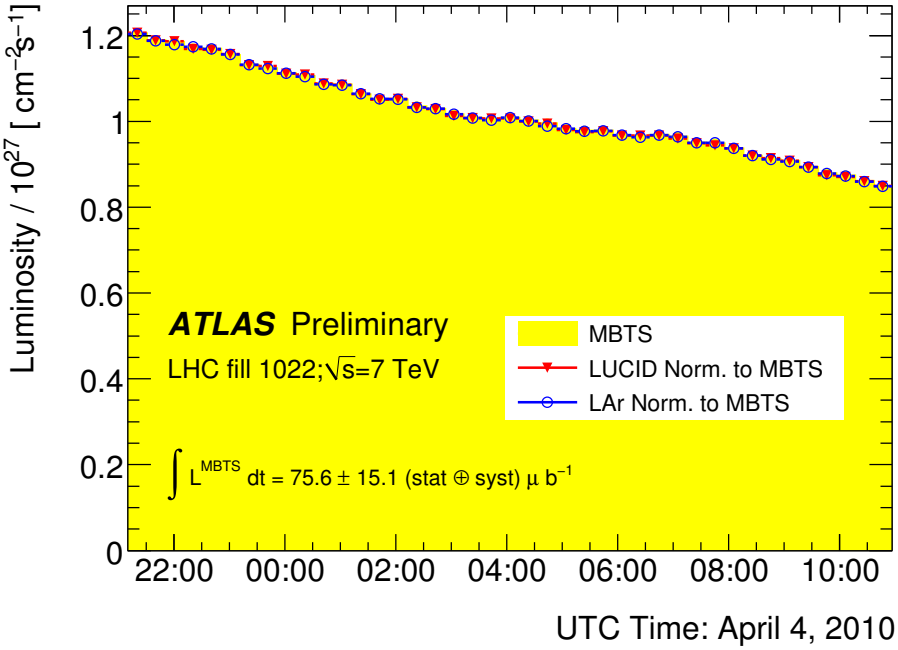

Figure 9: The ATLAS instantaneous luminosity as determined with the LAr (blue open circles) and the LUCID_Event_OR (open squares) normalized to the luminosity obtained using the MBTS (shaded area) for ATLAS run 152409, taken at $\sqrt{s} = 7$ TeV.

value of the effective beam height is, irrespective of the beam shape, equal to the area under the curve, divided by the ordinate at zero displacement.

Three sets of beam scans have been carried out in ATLAS, as detailed in Section 5.2. They were performed in both the horizontal (x) and the vertical (y) direction in order to fully reconstruct (under the assumption of negligible x-y coupling at the IP) the transverse convolved beam profile. During the scan, the collision rates measured by various ATLAS luminosity detectors were recorded while the beams were moved stepwise with respect to each other in the transverse plane. The principle of the luminosity calibration is to measure simultaneously the collision rate at zero beam separation, the charge of the colliding proton bunches and the horizontal and vertical convolved beam sizes [10].

5.1 The measurement of the luminosity

In terms of colliding beams parameters the luminosity $\mathscr{L}$ is defined as

$$\mathscr{L} = n_b f_r I_1 I_2 \int \rho_1(x,y)\rho_2(x,y)dxdy \tag{6}$$

where n_b is the number of colliding bunches, f_r is the machine revolution frequency (11245.5 Hz for LHC), $I_{1(2)}$ is the number of particles per bunch in beam 1 (2) and $\rho_{1(2)}(x,y)$ is the particle density in the transverse plane x-y of beam 1 (2) at the interaction point. Under the general assumption that there is no correlation between x and y, then the particle densities can be factorized and Equation 6 can be rewritten as

$$\mathscr{L} = n_b f_r I_1 I_2 \Omega_x(\rho_1(x)\rho_2(x))\Omega_y(\rho_1(y)\rho_2(y)) \tag{7}$$

where

$$\Omega_x(\rho_1,\rho_2) = \int \rho_1(x)\rho_2(x)dx$$

is the beam overlap integral in the x direction (with an analogous definition for the overlap integral in the y direction). In the method proposed by van der Meer in [9] the overlap integral (for example in the x direction) can be calculated as:

$$\Omega_x(\rho_1, \rho_2) = \frac{R_x(0)}{\int R_x(x)dx} \tag{8}$$

where $R_x(x)$ is the rate measured by a beam monitor detector during a horizontal beam scan when the beam separation is x. We define Σ_x by the equation:

$$\Sigma_x = \frac{1}{\sqrt{2\pi}} \frac{\int R_x(x)dx}{R_x(0)} \tag{9}$$

In the case that $R_x(x)dx$ is Gaussian, Σ_x coincides with the standard deviation of the rate distribution. By using the last two equations, Equation 7 can be rewritten as

$$\mathscr{L} = \frac{n_b f_r I_1 I_2}{2\pi \Sigma_x \Sigma_y} \tag{10}$$

which is a general formula to extract luminosity from machine parameters by performing a beam separation scan. Note that Equation 10 is quite general and does not dependent upon the shape of the experimental rate distribution versus beam separation (although it does depend on the assumption that there is no correlation between particle density distributions in x and in y).

5.2 Beam Scan Data Sets

Three van der Meer luminosity scans have been performed at the ATLAS interaction point. On April 26, 2010 a single scan in each of the horizontal and vertical planes was performed, while on May 9 two successive scans were performed.

The procedure for the beam scans [11] [12] is detailed below. After centering the beams on each other at the IP in both the horizontal and the vertical plane using mini-scans, a full-fledged luminosity-calibration scan was carried out in the horizontal plane, spanning a range of $\pm 6\sigma_b$ in horizontal beam-separation (where σ_b is the nominal transverse size of either beam at the IP). For the April scan, the relative transverse centering on the two beams was then verified using a miniscan in the horizontal plane, and found to be satisfactory. No such check was performed in the vertical. In the next step, a full-fledged luminosity-calibration scan was carried out in the vertical, again spanning a range of $\pm 6\sigma_b$ in relative beam separation.

The mini-scans used to first center the beams on each other in the transverse plane consist in activating closed-orbit bumps around the IP that vary the IP positions of both beams by $\pm 1\sigma_b$ in opposite directions, either horizontally or vertically. The relative positions of the two beams are then adjusted, in each plane, to achieve (at that time) optimum transverse overlap.

The full-fledged horizontal and vertical scans follow an identical procedure, where the same closed-orbit bumps are used to displace the two beams in opposite directions by $\pm 3\sigma_b$, resulting in a total variation of $\pm 6\sigma_b$ in relative displacement at the IP. This is illustrated in Figures 10, which displays the time-history of the relative horizontal separation of beams 1 and 2, called *nominal separation* and computed from the difference of the closed-bump amplitudes input to the LHC control system. In April, the horizontal scan started at zero nominal separation, moved to the maximum $B1 - B2$ separation in the negative direction, stepped back to zero and on to the maximum positive separation, and finally returned to the original settings of the closed-orbit bumps (zero nominal separation). The same procedure was followed for the vertical scan. In May, after collision optimization with the transverse miniscans, a full fledged horizontal scan was taken from negative to positive nominal separation, followed by a degaussing cycle where the horizontal nominal separation was run to $-6\sigma_b$, then 0 then $+6\sigma_b$, followed by a full

fledged horizontal scan in the opposite direction. The same procedure was then repeated in the vertical direction.

For each scan, at each of the 27 steps in relative displacement, the beams were left in a quiescent state for ~ 30 seconds, during which the (relative) luminosity measured by all active ATLAS luminosity monitors (*BCM*, *LUCID*, *MBTS* and *ZDC*)[4] was recorded as a function of time in a special purpose data stream, together with the value of the nominal separation, of the beam currents and of other relevant accelerator parameters transmitted to ATLAS by the accelerator control system. In addition, the full ATLAS data acquisition system was operational throughout the scan, using the standard ATLAS trigger menu, and triggered events were recorded as part of the normal data collection.

The full history of the raw luminosity is illustrated in Figure 11 (left). The luminosity was sampled every 1 to 2 seconds (depending on the subdetector), and is displayed here irrespective of whether the IP beam positions were left in the quiescent state (as required for valid luminosity measurements) or being adjusted between steps. Eliminating the samples corresponding to the non-quiescent state of the closed-orbit bumps, and averaging over the quiescent scan steps, yields the raw instantaneous luminosity over quiescent pseudo-luminosity blocks displayed in Figure 11 (right). Unless specifically stated otherwise, only the data points corresponding to steps 2 to 26 (Fig. 11, top) or 2 to 26 and 29 to 53 (Fig. 11, bottom), are retained in the analysis presented in the following sections.

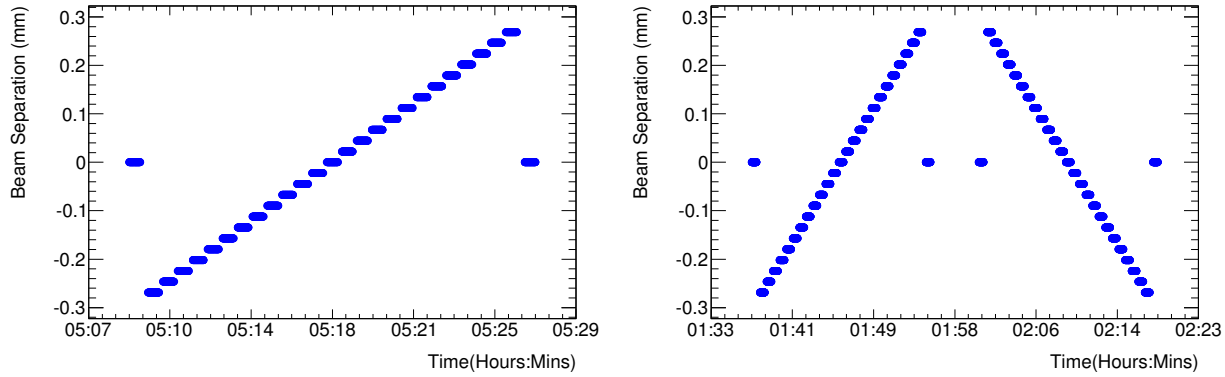

Figure 10: Scanning sequence for the full-fledged luminosity-calibration scans in the horizontal plane. Left: time-history of the horizontal nominal separation (computed from the difference in the closed-bump amplitudes as reported by the LHC control system) during the $vdM-I$ scan (26 Apr 2010). Right: same, for the $vdM-II$ and $vdM-III$ scans (9 May 2010). The horizontal axis is Geneva local time.

Variations of the number of protons per bunch during the beam scans were almost negligible. Changes of beam emittance resulting in variations of luminosity of a few per cent have been observed. The systematic uncertainty associated with this effect is discussed in Section 5.5. The main characteristics of the three scans are summarized in Table 5.

5.3 Parametrization and Analysis of the Beam Scan Data

Data from all three scans have been analyzed both from the dedicated data stream and from the standard ATLAS data stream. Because the dedicated stream recorded counting rates using the same detectors and algorithms as the OLC, this stream is appropriate for calibrating the online luminosity measurements.

[4] Analysis of data from the Beam Condition Monitors (BCM) [13] and Zero Degree Calorimeter (ZDC) [14] is in progress. No results on the calibration of these systems are reported in this note.

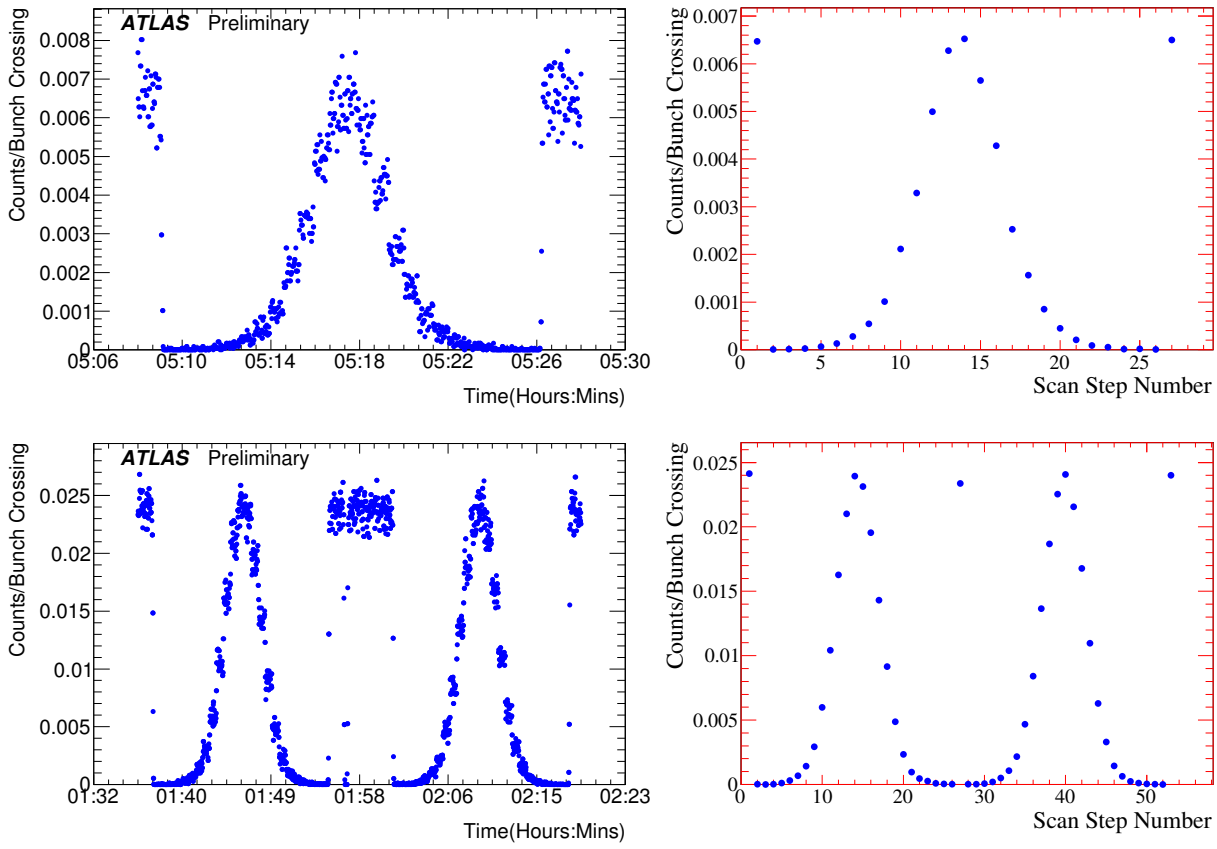

Figure 11: History of the raw luminosity, in units of events per bunch crossing, from the LUCID_Event_AND algorithm during full-fledged horizontal-calibration scans. Top: vdM-I scan (26 Apr 2010). Bottom: vdM-II and vdM-III scans (9 May 2010). Left: detailed time history of the sampled luminosity, irrespective of whether the transverse IP positions of the two beams were left in a quiescent state. Right: raw instantaneous luminosity averaged over those pseudo-luminosity blocks (or scan steps) where the IP positions were left unchanged; all steps are of equal duration. The points in steps 1 and 27 (top), and those in steps 1, 28 and 54 (bottom), correspond to closed-orbit bumps settings of zero nominal separation in both planes.

Actions	vdM Scan - I (April 26, 2010)	vdM Scan - II, III (May 9, 2010)
Scan Directions	1 horizontal scan followed by 1 vertical scan	2 horizontal scans followed by 2 vertical scans
Total Scan Steps/per plane	27 ($\pm 6\sigma$)	54 (27+27) ($\pm 6\sigma$)
Scan Duration/scan step	30 sec	30 sec
# of colliding bunches	1	1
Number of protons per colliding bunch	$\sim 0.09 \cdot 10^{11}$	$\sim 0.2 \cdot 10^{11}$
Typical luminosity/bunch (μb^{-1})	$0.5 \cdot 10^{-3}$	$1.7 \cdot 10^{-3}$
μ (interactions/crossing)	0.035	0.12
Luminosity Detectors Included	MBTS, Inner Detector, LUCID, BCM, ZDC	MBTS, Inner Detector LUCID , BCM, ZDC

Table 5: Summary of the main characteristics of the three beam scans performed in the ATLAS interaction point. Analysis of data from the BCM and ZDC has not yet been finalized.

Analyses using the standard ATLAS data stream suffer from reduced statistical precision relative to the dedicated stream, but allow for important cross-checks both of the background and of the size and position of the luminous region. In addition, because this stream contains full ATLAS events, these data can be used to measure the visible cross section corresponding to standard analysis selections that require, for example, timing cuts in the MBTS or Liquid Argon Calorimeter or the presence of a reconstructed primary vertex. Measurements performed using these two streams provide a consistent interpretation of the data within the relevant statistical and systematic uncertainties.

In all cases, the analyses fit the rate distributions as a function of beam separation to find Σ_x and Σ_y (defined in Equation 9). These results are then combined with a measurement of the beam intensities using Equation 10 to determine the luminosity. Although the mean number of interactions per crossing (μ) was low during the scans, the rates are corrected as a function of μ as described in Section 3.5. In addition, to remove sensitivity to beam lifetime effects which cause a decrease in beam current with time, the data are analyzed as *specific rates*, obtained by dividing the measured rate by the product of beam currents measured at that scan point:

$$R_{sp} = \frac{(I_1 I_2)_{MAX}}{(I_1 I_2)_{meas}} F(R_{meas}) \tag{11}$$

where $(I_1 I_2)_{meas}$ is the value of the product of the number of protons in the two colliding bunches during the measurement, $(I_1 I_2)_{MAX}$ is their maximum value during the scans (see Table 5), R_{meas} is the measured rate and $F(R_{meas})$ is the rate corrected for μ-dependent non-linearities.

Fits to the rate distributions require a choice of parametrization of the shape of the scan distribution. For all detectors and algorithms, fits using a single Gaussian or a single Gaussian with a flat background yield unacceptable χ^2 distributions. In all cases, fits to a Double Gaussian (with a common mean) plus a flat background result in χ^2 per degree of freedom close to one. In general, the background rates are consistent with zero for algorithms requiring a coincidence between sides, while small but statistically significant backgrounds are observed for algorithms requiring only a single side. These backgrounds are reduced to less than 0.3% of the luminosity at zero beam separation by using data from the paired bunches only. Offline analyses that require timing or a primary vertex in addition to being restricted to paired bunches, enjoy very low background. The residual is removed using the rate measured in unpaired bunches; no background term is therefore needed in the fit function for the offline case. Examples of such fits are shown in Figures 12 and 13. Figure 12 shows the fitted results for

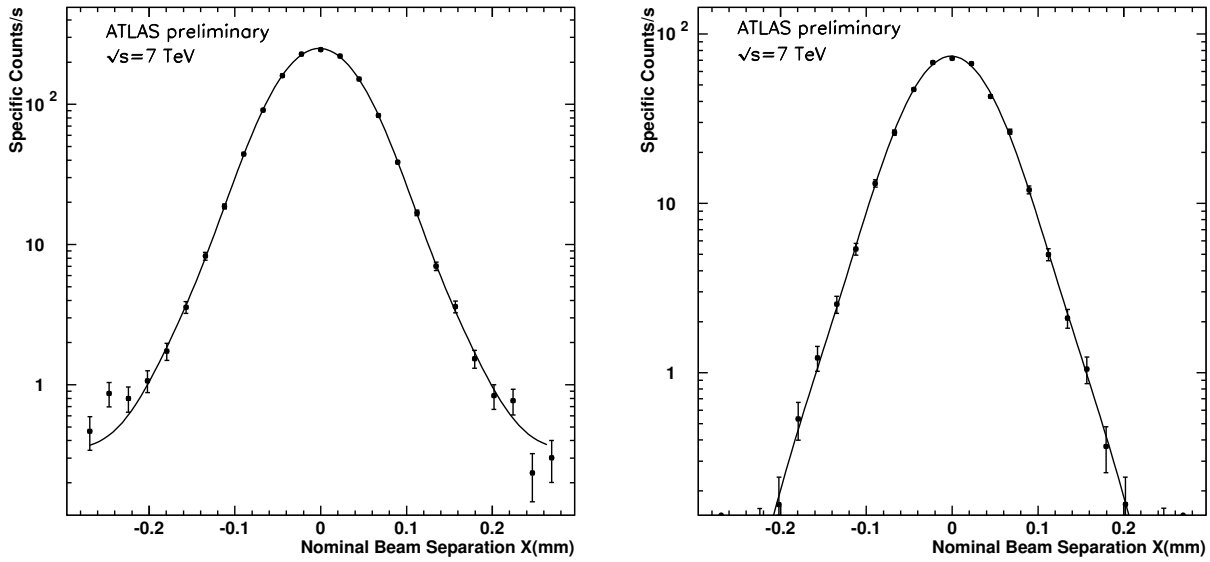

Figure 12: Results of the first luminosity scan in the horizontal direction for (left) the LUCID_Event_OR method (summed over both the colliding and the non-colliding BCID's), and (right) the LUCID_Event_AND method. The plots show the specific rate as a function of beam separation. Fits to a Double Gaussian with a common mean plus a constant background are superimposed.

the LUCID_Event_OR and LUCID_Event_AND algorithms for the first horizontal scan.[5)] The fits are displayed using a log scale for the rate to demonstrate that the background in the LUCID_Event_OR are well modeled by the fit. Figure 13 shows the fitted results for the first horizontal and vertical scans for the Primary Vertex Counting algorithm. These fits are displayed using a linear scale for the rate to demonstrate that the peak height and shape are well modeled by the fit.

In the case where the specific rate is described by a double Gaussian

$$R_x(x) = \frac{R_x(0)}{\sqrt{2\pi}} \left[\frac{f_a e^{-(x-x_0)^2/2\sigma_a^2}}{\sigma_a} + \frac{(1-f_a)e^{-(x-x_0)^2/2\sigma_b^2}}{\sigma_b} \right] \tag{12}$$

the value of Σ_x in Equation 10 is

$$\frac{1}{\Sigma_x} = \left[\frac{f_a}{\sigma_a} + \frac{1-f_a}{\sigma_b} \right] \tag{13}$$

5.4 Fit Results

A summary of the relevant fit parameters for the three beam scans is presented in Table 6. Results are provided for four online algorithms (LUCID_Event_AND, LUCID_Event_OR, L1_MBTS_1_paired and L1_MBTS_1_1_paired) and two offline algorithms (MBTS_1_timing and Primary Vertex Counting). Examination of this table indicates that the results for the mean position and Σ for a given scan are consistent within statistical uncertainties among algorithms. These results also indicate several potential sources of systematic uncertainty. First, the fitted position (in units of beam separation) of the peak luminosity deviates from zero by as much as 7 μm, indicating that the beams may not have been properly

[5)] For scan 1, a single tube in LUCID was not functional. Efficiencies have been corrected for this effect.

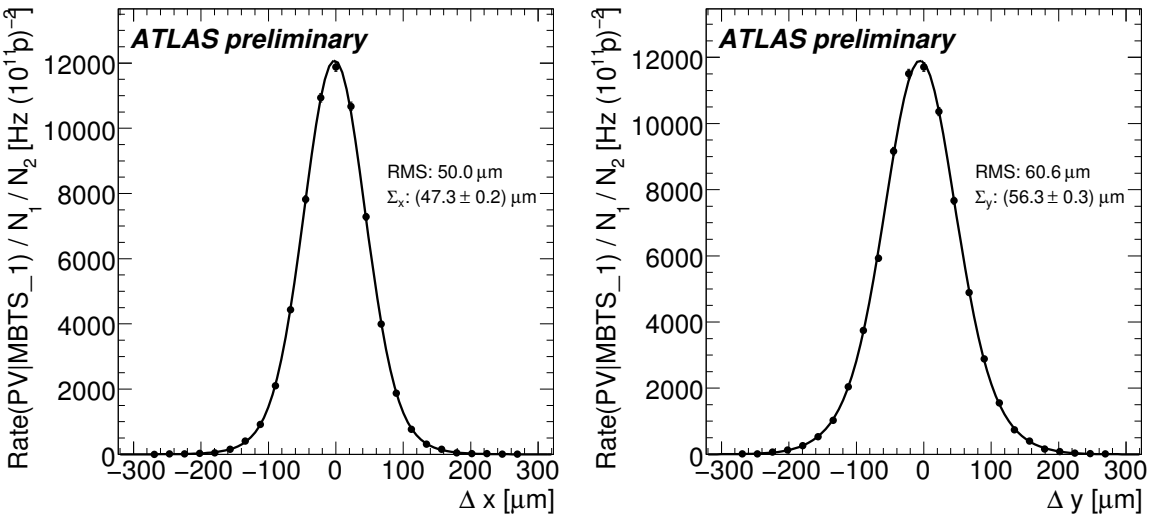

Figure 13: Results of the first luminosity scan in the horizontal (left) and vertical (right) plane for the Primary Vertex Counting method. The plots show the specific rate per $10^{22}(\text{protons/bunch})^2$ as a function of beam separation. Double Gaussian fits with a common mean are superimposed, together with the resulting values for Σ_x and Σ_y (defined in Equation 9).

centered before the start of the scan. Second, in scans 2 and 3, the peak rates for the horizontal and vertical scans, as measured with a single algorithm, show a systematic difference of as much as 5% (with a lower rate observed in the vertical scan for all algorithms). This systematic dependence may indicate a level of irreproducibility in the scan setup. The effect of these systematic uncertainties on the luminosity calibration is discussed in Section 5.5.

Calibration of the absolute luminosity from the beam scans uses the following expression for σ_{vis}:

$$\sigma_{vis} = \frac{R^{MAX}}{\mathscr{L}_p} = R^{MAX}\frac{2\pi\Sigma_x\Sigma_y}{n_b f_r I_1 I_2} \tag{14}$$

where R^{MAX} and L_p are, respectively, the specific rate and the luminosity measured when the beams collide exactly head-on. Since there are two independent measurements, one each for the x and y directions, and each has the same statistical significance, the average of the two measurements is considered as the best estimate of R^{MAX}:

$$R^{MAX} = \frac{1}{2}(R_x^{MAX} + R_y^{MAX}) \tag{15}$$

The values of σ_{vis} for each method and each scan are reported in Table 7. While the results of the second and third luminosity scans are compatible within statistical uncertainties, those of the first luminosity scan are lower by 2.7 to 4.8% for all algorithms (except Primary Vertex Counting). These differences again indicate possible systematic variations occurring between machine fills.

Table 7 also reports the specific luminosity normalized to units of 10^{11} protons per bunch

$$\mathscr{L}_{spec} = 10^{22}(\text{p/bunch})^2\frac{f_r}{2\pi\Sigma_x\Sigma_y} \tag{16}$$

Because the emittance of Scan 1 was different from that of Scans 2 and 3, the specific luminosity of that scan is not expected to be the same. The agreement between algorithms within one scan is excellent. This agreement demonstrates that the variations in the measured value of σ_{vis} with scan number for a given algorithm is due to variations in the fitted rate R^{MAX} rather than in the values obtained for Σ.

Algorithm	Mean Position (μm)	Σ (μm)	Background (Hz)	R^{MAX} (Hz)	χ^2/DOF
Horizontal Scan 1					
LUCID_Event_AND	-1.12 $\pm$ 0.46	47.40 $\pm$ 0.56	0.01 $\pm$ 0.04	75.6 $\pm$ 1.1	0.9
LUCID_Event_OR	-1.58 $\pm$ 0.25	47.27 $\pm$ 0.29	0.06 $\pm$0.04	247.8 $\pm$ 2.0	0.5
L1_MBTS_1_1_paired	-1.85 $\pm$ 0.25	47.33 $\pm$ 0.25	0.03 $\pm$ 0.04	319.0 $\pm$ 2.3	0.8
L1_MBTS_1_paired	$-$2.05$\pm$ 0.24	47.30 $\pm$ 0.26	1.01 $\pm$ 0.11	361.7 $\pm$ 2.6	1.0
MBTS_1_timing	$-$1.66 $\pm$ 0.26	47.05 $\pm$ 0.26	N/A	306.8 $\pm$ 1.6	1.0
Primary Vertex Counting	$-$1.7$\pm$ 0.2	47.26 $\pm$ 0.25	N/A	329.7 $\pm$ 1.6	0.8
Vertical Scan 1					
LUCID_Event_AND	-5.04 $\pm$ 0.50	55.52 $\pm$ 0.59	0.05 $\pm$ 0.03	75.8 $\pm$ 1.0	0.8
LUCID_Event_OR	-5.23 $\pm$ 0.28	55.28 $\pm$ 0.33	0.16 $\pm$ 0.06	246.2 $\pm$ 1.9	1.1
L1_MBTS_1_1_paired	-5.24 $\pm$ 0.28	55.73 $\pm$ 0.30	0.10 $\pm$ 0.06	318.5 $\pm$ 2.3	1.2
L1_MBTS_1_paired	-5.25 $\pm$ 0.26	55.82 $\pm$ 0.28	1.08 $\pm$ 0.12	359.2 $\pm$ 2.5	1.2
MBTS_1_timing	$-$5.53 $\pm$ 0.30	56.32 $\pm$ 0.29	N/A	297.8 $\pm$ 1.4	2.1
Primary Vertex Counting	$-$5.17 $\pm$ 0.26	56.28 $\pm$0.30	N/A	323.0 $\pm$ 1.5	1.1
Horizontal Scan 2					
LUCID_Event_AND	7.65 $\pm$ 0.25	58.78 $\pm$ 0.16	-0.02 $\pm$ 0.06	265.4 $\pm$ 3.0	1.8
LUCID_Event_OR	7.41 $\pm$ 0.14	58.76 $\pm$ 0.08	0.07 $\pm$ 0.12	858.9 $\pm$ 2.5	2.0
L1_MBTS_1_1_paired	7.28 $\pm$ 0.13	59.06 $\pm$ 0.09	-0.28 $\pm$ 0.16	1107.3 $\pm$ 3.1	0.9
L1_MBTS_1_paired	7.30 $\pm$ 0.13	58.93 $\pm$ 0.09	1.04 $\pm$ 0.25	1253.1 $\pm$ 3.6	1.2
MBTS_1_timing	7.44 $\pm$ 0.22	58.71 $\pm$ 0.23	N/A	1087.0 $\pm$ 4.1	1.3
Primary Vertex Counting	7.56 $\pm$ 0.20	58.63 $\pm$ 0.21	N/A	1133.0 $\pm$ 4.0	1.1
Vertical Scan 2					
LUCID_Event_AND	1.99 $\pm$ 0.27	62.75 $\pm$ 0.93	-0.21 $\pm$ 0.14	253.8 $\pm$ 2.9	1.6
LUCID	1.99 $\pm$ 0.16	62.37 $\pm$ 0.16	0.13 $\pm$ 0.13	825.3 $\pm$ 3.1	0.8
L1_MBTS_1_1_paired	2.17 $\pm$ 0.15	62.18 $\pm$ 0.16	0.30 $\pm$ 0.15	1068.9 $\pm$ 3.9	0.9
L1_MBTS_1_paired	2.11 $\pm$ 0.15	62.13 $\pm$ 0.15	1.70 $\pm$ 0.20	1207.6 $\pm$ 4.2	1.0
MBTS_1_timing	2.22 $\pm$ 0.24	62.61 $\pm$ 0.27	N/A	1038.0 $\pm$ 3.8	1.5
Primary Vertex Counting	2.09 $\pm$ 0.21	62.48 $\pm$ 0.25	N/A	1081.0 $\pm$ 3.6	0.9
Horizontal Scan 3					
LUCID_Event_AND	5.48 $\pm$ 0.26	58.94 $\pm$ 0.97	0.04 $\pm$ 0.13	266.8 $\pm$ 3.0	1.2
LUCID_Event_OR	5.66 $\pm$ 0.15	58.57 $\pm$ 0.18	0.42 $\pm$ 0.10	856.8 $\pm$ 3.3	2.1
L1_MBTS_1_1_paired	5.59 $\pm$ 0.14	58.88 $\pm$ 0.10	0.15 $\pm$ 0.14	1102.5 $\pm$ 3.2	2.3
L1_MBTS_1_paired	5.59 $\pm$ 0.14	58.87 $\pm$ 0.33	1.20 $\pm$ 0.30	1244.4 $\pm$ 7.8	2.5
MBTS_1_timing	6.02 $\pm$ 0.22	59.05 $\pm$ 0.23	N/A	1074.0 $\pm$ 4.0	0.95
Primary Vertex Counting	5.95 $\pm$ 0.20	59.14 $\pm$ 0.23	N/A	1120.0 $\pm$ 3.8	1.4
Vertical Scan 3					
LUCID_Event_AND	-0.01 $\pm$ 0.27	62.21 $\pm$ 0.30	-0.03 $\pm$ 0.08	259.9 $\pm$ 2.9	0.9
LUCID_Event_OR	0.08 $\pm$ 0.16	62.06 $\pm$ 0.16	0.23 $\pm$ 0.12	830.2 $\pm$ 3.1	0.8
L1_MBTS_1_1_paired	0.04 $\pm$ 0.15	62.09 $\pm$ 0.16	0.15 $\pm$ 0.15	1075.6 $\pm$ 3.9	1.2
L1_MBTS_1_paired	0.06 $\pm$ 0.15	62.09 $\pm$ 0.15	1.65 $\pm$ 0.22	1214.5 $\pm$ 4.2	1.1
MBTS_1_timing	$-$0.16 $\pm$ 0.24	61.45 $\pm$ 0.30	N/A	1056.0 $\pm$ 4.0	1.4
Primary Vertex Counting	$-$0.06 $\pm$ 0.21	61.83 $\pm$ 0.27	N/A	1102.0 $\pm$ 3.7	1.4

Table 6: Summary of the relevant fit parameters for the three beam Scans. Results are presented for four online algorithms (LUCID_Event_AND, LUCID_Event_OR, L1_MBTS_1_1_paired and L1_MBTS_1_paired) and for two offline algorithms (MBTS_1_timing and Primary Vertex Counting).

Method	Scan Number	σ_{vis} mb	$\mathscr{L}_{spec}$ (10^{29} cm^{-2}s^{-1})
LUCID_Event_AND	1	12.15 ± 0.14	6.80 ± 0.08
	2	12.55 ± 0.10	4.85 ± 0.03
	3	12.73 ± 0.10	4.88 ± 0.09
LUCID_Event_OR	1	39.63 ± 0.32	6.85 ± 0.06
	2	40.70 ± 0.13	4.88 ± 0.01
	3	40.77 ± 0.14	4.92 ± 0.02
L1_MBTS_1_1_paired	1	51.14 ± 0.39	6.78 ± 0.05
	2	52.59 ± 0.16	4.87 ± 0.01
	3	52.64 ± 0.16	4.90 ± 0.02
L1_MBTS_1_paired	1	57.83 ± 0.43	6.79 ± 0.05
	2	59.47 ± 0.18	4.89 ± 0.01
	3	59.43 ± 0.25	4.90 ± 0.02
MBTS_1_timing	1	49.28 ± 0.31	6.76 ± 0.05
	2	51.64 ± 0.23	4.87 ± 0.03
	3	51.29 ± 0.24	4.93 ± 0.03
Primary Vertex Counting	1	53.48 ± 0.29	6.73 ± 0.05
	2	53.64 ± 0.22	4.89 ± 0.03
	3	53.78 ± 0.23	4.89 ± 0.02

Table 7: Measurement of the visible cross section and peak specific luminosity for four online algorithms (LUCID event AND, LUCID event OR, L1_MBTS_1_1_paired and L1_MBTS_1_paired) and two offline algorithms (MBTS_1_timing and Primary Vertex Counting) for each of the three beam scans. The uncertainties reported here are statistical only. The emittance of Scan 1 was different from that of Scans 2 and 3, so the specific luminosity of that scan is not expected to be the same.

5.5 Systematic Uncertainties

Systematic uncertainties affecting the luminosity and visible cross section measurements arise from the following effects.

1. **Beam intensities**

   Any systematic error affecting the measurement of absolute bunch charge translates directly into an uncertainty on the calculated luminosity scale. The LHC instrumentation experts have therefore attempted to ensure that the bunch-intensity information associated with the luminosity-calibration scans is as accurate as possible. The raw bunch-by-bunch intensity information logged in the database was corrected in two steps [15].

   The fast BCT [16] measures the total charge contained in 25 ns-long time slots nominally centered on the circulating bunches. Small timing errors and imperfections in the transformer response may result in a few percent of the total bunch signal appearing in the time slot adjacent to that of the bunch under consideration. This is an instrumental effect and does not imply that protons themselves diffused into the corresponding RF buckets. The first step of the recalibration process therefore consists in adding back to the correct time slot, the charge originally reported in the neighboring one; this correction typically amounts to a 2-5% effect.

   Next, the total circulating charge (summed over both colliding and non-colliding bunches) reported by the fast BCT, is rescaled to the total-current measurement of the DCCT [16]. This is based on the assumption that the error introduced by an eventual debunched-beam component (which is not detectable by the fast BCT) is negligible at these intensities ($\sim$ 1-2 $\times 10^{10}$ protons per bunch and 2-4 $\times 10^{10}$ protons per beam). This rescaling is motivated by the fact that the DCCT, which uses much slower electronics and no internal digital processing, is easier to tune and calibrate than the BCT. Its poorer noise performance (compared to that of the fast BCT) is not an issue when the measurements are averaged over tens of seconds.

   The overall correction applied to the original bunch-current data amounts to 13% on the bunch-charge product for scan I, and to 9% for scans II+III. The reason for these large corrections is not fully understood yet, but is suspected to be associated with the calibration system and calibration procedure of the fast BCT.

   At these intensities, the uncertainty on the corrected bunch intensity is believed to be dominated by that on the overall accuracy of the DCCT. While laboratory measurements show that its absolute scale accuracy is better than 2%, the DCCT suffers from slow baseline drifts (a known issue for this type of instrument), that are beam-, time- and temperature-dependent. These baseline offsets can only be determined with no beam in the LHC. For the fills under consideration, the DCCT baseline was measured before injection, and then again after dumping the beam. Each of those measurements is affected by an equivalent peak-to-peak (or "envelope") uncertainty of $\pm 1 \times 10^9$ protons in total beam intensity, which is conservatively translated into a peak-to-peak uncertainty of $\pm 2 \times 10^9$ protons on the total beam current reported by the DCCT during the fill. Other potential sources of measurement error are under study [17], but are thought to be negligible at these low bunch intensities and small number of bunches, where the error is dominated by the absolute scale accuracy and by the baseline drifts of the DCCT.

   Taking into account the impact of these two main components, leads to the following estimate of the uncertainty on the measured bunch intensity I_B:

$$\Delta I_B / I_B = \pm [2 \times 10^9 / (N \times I_B) + 0.02]$$

where ΔI_B is the peak-to-peak uncertainty on I_B, N is the total number of bunches per beam, and I_B is the bunch charge corrected as described above. The first term in the above equation reflects the uncertainty associated with the DCCT baseline subtraction, and the second term that on the absolute DCCT scale. It should be stressed that ΔI_B is a peak-to-peak or 'tolerance' uncertainty, in the sense that it covers the full possible range of measurement errors; in other words, the true value of I_B may lie anywhere in the interval $I_B \pm \Delta I_B$, but not outside. Interpreting ΔI_B as a 1-σ error would therefore be an overestimate. Under the assumption of a uniform error distribution of half width $\Delta I_B/I_B$, the fractional 1-σ uncertainty can be estimated by

$$\sigma(I_B)/I_B = [\Delta I_B/I_B]/\sqrt{3} = [2\times 10^9/(N\times I_B)+0.02]/\sqrt{3}$$

This leads, for example, to a bunch-charge uncertainty of $\sigma(I_B)/I_B = 6.9\%$ in the case of a beam with two circulating bunches containing 1×10^{10} protons each, or $\sigma(I_B)/I_B = 4.0\%$ in the case of two circulating bunches of 2×10^{10} protons each.

A more precise quantitative characterization of these errors and of their degree of correlation between the two beams is still in progress. Conservatively treating the current-scale uncertainty as fully correlated between the two beams, results in a total systematic error of $\pm 14\%$ on the product of bunch currents for vdM scan I, and $\pm 8\%$ for scans II and III. Because the baseline correction dominates the overall bunch-charge uncertainty and because it drifts on the time scale of a few hours, these uncertainties are largely uncorrelated between the first (scan I) and the second (scans II+III) luminosity-calibration sessions. Taking into account the bunch currents listed in Table 5 leads to an (unweighted) average uncertainty of $\sigma(I_B)/I_B = 4\%$ for each beam, or 8% on the overall luminosity scale. In view of the preliminary nature of these error estimates, this number has been rounded up to an overall uncertainty of $\sigma(I_B)/I_B = 10\%$ on the bunch-current product. This 10% uncertainty on the beam-current product is by far the largest systematic uncertainty on the luminosity calibration.

2. **Length scale calibration**
The desired nominal beam separation during beam scans determines the magnet settings of the closed orbit bumps that generate the beam separation. The only accelerator instrumentation available for calibrating the length scale of the beam separation is the beam position monitor system. Unfortunately, the short-term stability and reliability of this system are not adequate to perform such a calibration. In contrast, the vertex resolution of the ATLAS inner detector provides a stable and reliable method of calibration. These calibrations were done in dedicated scans where both beams were moved in the same direction first by $+100$ μm and then by -100 μm from the nominal beam position first in the horizontal and then in the vertical direction. The luminous beam centroid was determined using reconstructed primary vertices. In addition, the primary vertex event rate was monitored to ensure that the two beams remained centered with respect to each other. The calibration constants derived for the length scale were (1.001 ± 0.003) and (1.001 ± 0.004) in the horizontal and vertical directions respectively, indicating that the scale associated with the magnet settings and that obtained from the ATLAS inner detector agree to better than 0.5%. It should be noted that if the profiles of the two beams do not have the same width, the measured centroid of the luminous region will vary systematically as a function of beam separation. This possibility has been considered and is included in the quoted systematic uncertainty on the length scale. In addition, it should be noted that the length scale calibration scans consisted of only three points and extended to only ± 100 μm, these data do not allow for studies of non-linearities or studies of the calibration at large beam displacements. Because of these concerns, a systematic uncertainty of 2% is assigned to length scale calibration in spite of the high precision of the calibration scan data.

3. **Effect of Imperfect Beam Centering**
   If the beams are slightly offset with respect to each other in the scan direction, there is no impact on the results of the luminosity scan. However, a deviation from zero separation in the transverse direction orthogonal to that of the scan reduces the rate observed for all the data points of that scan. The systematic uncertainty associated with imperfect beam centering has been estimated by considering the maximum deviation of the peak position (measured in terms of the nominal beam separation) from the nominal null separation that was calibrated through the re-alignment of the beams at the beginning of that scan. This deviation is translated into an expected decrease in rate and therefore in a systematic uncertainty affecting the measurement of the visible cross section. A systematic uncertainty of 2% is assigned.

4. **Transverse Emittance Growth and Other Sources of Non-reproducibility**
   Wire-scanner measurements of the transverse emittances of the LHC beams were performed at regular intervals during the luminosity-scan sessions, yielding measured emittance degradations of roughly 5-10% per beam and per plane between the beginning and the end of the luminosity-calibration sessions [18]. This emittance growth causes a progressive increase of the transverse beam sizes (and therefore of Σ_x and Σ_y), leading to a $\sim 2\%$ degradation of the specific luminosity between the first and the last scan within one session. This luminosity degradation, in turn, should be reflected in a variation, over time, of the specific rates R_x^{MAX} and R_y^{MAX} (Eq. 15). A first potential bias arises because if the time dependence of Σ_x and Σ_y during a scan is not taken into account, the emittance growth may effectively distort the luminosity-scan curve. Next, and because the horizontal and vertical scans were separated in time, uncorrected emittance growth may induce inconsistencies in computing the luminosity from accelerator parameters using Eq. 14. The emittance growth was estimated independently from the wire-scanner data, and by a technique that relies on the relationship, for Gaussian beams, between Σ, the single-beam sizes σ_1 and σ_2 and the transverse luminous size σ_L (which is measured using the spatial distribution of primary vertices) [10]:

$$\begin{aligned} \Sigma &= \sqrt{\sigma_1^2 + \sigma_2^2} \\ \frac{1}{\sigma_L} &= \sqrt{\left(\frac{1}{\sigma_1^2} + \frac{1}{\sigma_2^2}\right)} \end{aligned}$$

   Here the emittance growth is taken from the measured evolution of the transverse luminous size during the fill. The variations in both Σ and R^{MAX} (which should in principle cancel each other when calculating the luminosity) were then predicted from the two emittance-growth estimates, and compared to the luminosity-scan results. While the predicted variation of Σ, between consecutive scans, is very small (0.3 - 0.8 μm) and well reproduced by the data, the time evolution of R^{MAX} displays irregular deviations from the wire-scanner prediction of up to 3%, suggesting that at least one additional source of non-reproducibility is present. Altogether, these estimates suggest that a $\pm 3\%$ systematic uncertainty on the luminosity calibration be assigned to emittance growth and unidentified causes of non-reproducibility.

5. **μ Dependence of the Counting Rate**
   All measurements have been corrected for μ dependent non-linearities. Systematic uncertainties on the predicted counting rate as a function of μ have been studied using Monte Carlo simulations, where the efficiency (or equivalently σ_{vis}) have been varied. For $\mu < 2$ the uncertainty is estimated to be $< 2\%$.

Source	Uncertainty on σ_{vis} (%)
Beam Intensities	10
Length Scale Calibration	2
Imperfect Beam Centering	2
Transverse Emittance Growth & Other Sources of Non-Reproducibility	3
μ Dependence	2
Total	11

Table 8: Summary of systematic uncertainties on the visible cross sections obtained from beam scans. Because σ_{vis} is used to determine the absolute luminosity (see Equation 1), these results are also the systematic uncertainty on the beam-scan based luminosity calibrations.

Algorithm	σ_{vis}^{meas} (mb)	σ_{vis}^{PYTHIA} (mb)	$\frac{\sigma_{vis}^{PYTHIA}}{\sigma_{vis}^{meas}}$	σ_{vis}^{PHOJET} (mb)	$\frac{\sigma_{vis}^{PHOJET}}{\sigma_{vis}^{meas}}$
LUCID_Event_AND	$12.4 \pm 0.1 \pm 1.4$	15.7	1.27	16.8	1.35
LUCID_Event_OR	$40.2 \pm 0.1 \pm 4.4$	46.7	1.16	53.4	1.32
L1_MBTS_1_1_paired	$51.9 \pm 0.2 \pm 5.7$	58.4	1.13	68.7	1.32
L1_MBTS_1_paired	$58.7 \pm 0.2 \pm 6.5$	66.6	1.14	73.7	1.26
MBTS_1_timing	$50.4 \pm 0.2 \pm 5.7$	57.6	1.14	67.8	1.35
Primary Vertex Counting	$53.6 \pm 0.2 \pm 5.9$	57.9	1.08	70.0	1.31

Table 9: Comparison of the visible cross sections determined from beam scans (σ_{vis}^{meas}) to the predictions of the PYTHIA and PHOJET Monte Carlo generators. The ratio of predictions to measurements is also shown. Note that the systematic uncertainty on the measurements are 100% correlated among the methods.

A summary of the systematic uncertainties is given in Table 8. The overall uncertainty of 11% is dominated by the measurement of the beam intensities. At least some portion of this uncertainty is common to all interaction points at the LHC. The size of this correlated uncertainty with respect to other experiments has not yet been evaluated.

As noted above, there is a systematic difference between σ_{vis} obtained in the first scan from that obtained in the second and third scans. In reporting a best estimate of the σ_{vis}, we have chosen to average the value obtained in the first scan with the average value of the second and third. These values for the visible cross section are reported in Table 9, together with the predictions of PYTHIA (ATLAS MC09 tune) and PHOJET. The measurements of the visible cross sections are lower than the PYTHIA (PHOJET) predictions by 8% to 27% (26% to 35%).

The method-to-method variations in the ratio of σ_{vis} measured in the beam scans to that predicted by Monte Carlo generators are consistent with the detector-dependent systematic uncertainties given in Table 4 for all methods except LUCID_Event_AND. Given the 11% (fully correlated) systematic uncertainty on the luminosity measurements obtained from the beam scans and the $\sim 5\%$ detector-dependent systematic uncertainties listed in Table 4, it is impossible to know whether the disagreement with PYTHIA MC09 is the result of inaccuracies in the PYTHIA model or of a systematic error on the measurement of the beam current. Given the quoted uncertainties, the agreement with PHOJET is marginal.

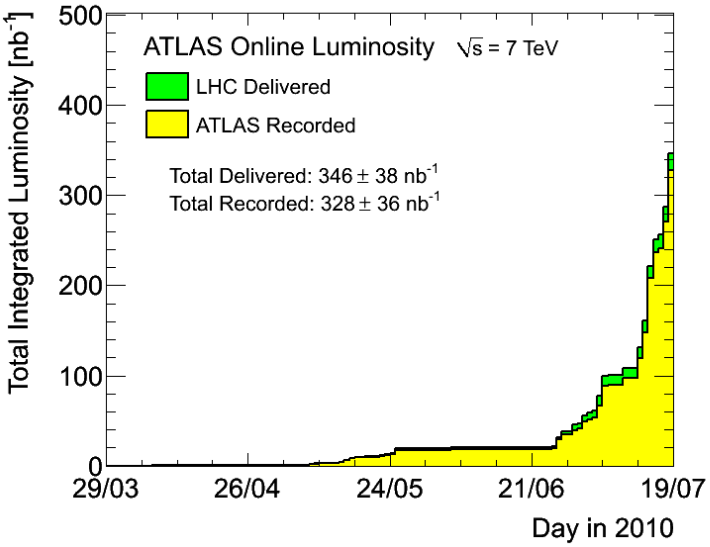

Figure 14: Cumulative integrated luminosity versus day delivered to (green), and recorded by ATLAS (yellow) during stable beams and for 7 TeV centre-of-mass energy. The luminosity calibration uses the van der Meer scan results from the LUCID_Event_OR algorithm.

5.6 Choice of Preferred Algorithm

The results of the previous section indicate that all the luminosity algorithms give consistent measurements of the specific luminosity. In addition, all show similar levels of consistency between the different scans, and (except for LUCID_Event_AND) between Monte Carlo and beam-scan calibrations. These data, therefore, do not point to a unique choice for a preferred luminosity algorithm. ATLAS has decided to use the LUCID_Event_OR algorithm as its baseline choice, at this time, for offline luminosity determination. Several factors have contributed to this decision. First, the LUCID detector was designed to provide robust luminosity measurements for ATLAS up to luminosities above 10^{34} cm^{-2}s^{-1}; in contrast, the MBTS is expected to undergo radiation damage when luminosities exceed 10^{33} cm^{-2}s^{-1}. Second, the LUMAT card provides luminosity information that is independent of the ATLAS data acquisition system (TDAQ): LUCID is therefore less sensitive to TDAQ downtime than the other detectors. Third, the background in LUCID is low even for the single sided LUCID_Event_OR algorithm. At low luminosity, LUCID_Event_OR has better statistical precision than LUCID_Event_AND. At high luminosity, the dependence on μ is smaller and has a less complicated dependence. Figure 14 shows the total delivered (recorded) luminosity versus day (through 19 July 2010) obtained using LUCID_Event_OR as the preferred algorithm.

6 Conclusions

Measurements of the LHC luminosity have been performed at $\sqrt{s} = 900$ GeV and $\sqrt{s} = 7$ TeV using several detectors and methods. These methods track relative luminosities to within their statistical uncertainties. Absolute luminosity calibration obtained using Monte Carlo determined efficiencies are limited to $\sim 20\%$ by the systematic uncertainty associated with the modeling of the diffractive components of the pp cross section, as well as by detector-specific systematic uncertainties that are typically of order 5% .

Absolute luminosity calibration obtained from van der Meer beam scans at $\sqrt{s} = 7$ TeV have a systematic uncertainty of 11% which is dominated by the uncertainty in the bunch intensities. The visible cross sections obtained from the beam scans are lower than those predicted by PYTHIA MC09 (PHOJET) by 8% to 27% (26% to 35%).

References

[1] G. Aad et al., ATLAS Collaboration, JINST **3** (2008) S08003.

[2] G. Aad et al., ATLAS Collaboration, Physics Letters B **688** (2010) 21–42.

[3] G. Aad, et al., ATLAS Collaboration, ATLAS Monte Carlo Tunes for MC09, ATLAS-PHYS-PUB-2010-002, 2010.

[4] ATLAS Collaboration, Charged particle multiplicities in pp interactions at $\sqrt{s} = 7$ TeV measured with the ATLAS detector at the LHC, ATLAS-CONF-2010-024, 2010.

[5] Vaia Papadimitriou, NIM **598** (2008) 14–18.

[6] S. Klimenko, J. Konigsberg, T. Liss, Averaging of the inelastic cross sections measured by the CDF and the E811 experiments, Fermilab-FN-0741 and references therein, 2003.

[7] ATLAS Collaboration, ATLAS Forward Detectors for Measurement of Elastic Scattering and Luminosity, CERN,LHCC/2008-004.

[8] C. Anastasiou, L. Dixon, K. Melnikov, and F. Petriello, Phys. Rev. **D69** (2004) 94008.

[9] S. van der Meer, CERN-ISR-PO-68-31, 1968.

[10] ATLAS Collaboration, Characterization of Interaction-Point Beam Parameters Using the pp Event-Vertex Distribution Reconstructed in the ATLAS Detector at the LHC, ATLAS-CONF-2010-027, 2010.

[11] H. Burkhardt and P. Grafstrom, Absolute Luminosity From Machine Parameters, LHC-PROJECT-Report-1019, 2007.

[12] S.M. White, R. Alemany-Fernandez, H. Burkhardt, M. Lamont, First Luminosity Scans in the LHC, http://accelconf.web.cern.ch/AccelConf/IPAC10/papers/mopec014.pdf, 2010.

[13] V. Cindro et al., JINST **3** (2008) P02004.

[14] S. White, NIM **617** (2009) 126–128.

[15] J. J. Gras, Private Communication (June 2010).

[16] D. Belohrad, J-J. Gras, L. K. Jensen, O. R. Jones, M. Ludwig, P. Odier, J. J. Savioz, S. Thoulet, Commissioning and First Performance of the LHC Beam Current Measurement Systems, http://accelconf.web.cern.ch/AccelConf/IPAC10/papers/mope059.pdf.

[17] J. J. Gras et al, LHC note in preparation.

[18] Data courtesy of S. M. White.